The Role of Mesenchymal Cells in Cholangiocarcinoma

Mireia Sueca-Comes[1,*], Elena Cristina Rusu[2], Jennifer C. Ashworth[1,3], Pamela Collier[1], Catherine Probert[1], Alison Ritchie[1], Marian Meakin[1], Nigel P. Mongan[3,5], Isioma U. Egbuniwe[1], Jesper Bøje Andersen[4], David O. Bates[1], Anna M. Grabowska[1]

[1]Translational Medical Science, School of Medicine, Biodiscovery Institute, University of Nottingham
[2]Institute of Integrative Systems Biology (I2Sysbio), University of Valencia and CSIC
[3]School of Veterinary Medicine and Science, Sutton Bonington Campus, Leicestershire, LE12 5RD
[4]Biotech Research and Innovation Centre (BRIC), Department of Health and Medical Sciences, University of Copenhagen, Copenhagen
[5]Department of Pharmacology, Weill Cornell Medicine, 10065, NY, USA

*Corresponding author: Mireia Sueca-Comes:
Email: m.sueca95@gmail.com

Keywords: Cholangiocarcinoma; PDX models; mesenchymal stem cells, signalling pathways; tumour microenvironment.

Abstract

The tumour microenvironment (TME) significantly influences tumour formation and progression through dynamic interactions. Cholangiocarcinoma (CCA), a highly desmoplastic tumour, lacks early diagnostic biomarkers and has limited effective treatments due to an incomplete understanding of its molecular pathogenesis. Investigating the TME's role in CCA progression could lead to better therapies.

RNA sequencing was performed on seven CCA PDXs and their corresponding patient samples. Differential expression analysis was conducted, and Qiagen Ingenuity Pathway Analysis (IPA) was used to predict dysregulated pathways and upstream regulators. PDX and cell line-derived spheroids, with and without immortalised mesenchymal stem cells, were grown and analysed for morphology, growth, and viability. Histological analysis confirmed biliary phenotypes. RNA sequencing indicated upregulation of ECM-receptor interaction and PI3K-Akt pathways in the presence of MSCs, with several genes linked to poor survival. MSCs restored the activity of inhibited cancer-associated kinases (ICAKs).

This study shows that adding MSCs to CCA spheroid models restores key paracrine signalling pathways lost in PDXs, enhancing tumour growth and viability. These findings

© 2024. Published by The Company of Biologists Ltd.
This is an Open Access article distributed under the terms of the Creative Commons Attribution License (http://creativecommons.org/licenses/by/4.0), which permits unrestricted use, distribution and reproduction in any medium provided that the original work is properly attributed

Disease Models & Mechanisms • DMM • Accepted manuscript

highlight the importance of including stromal components in cancer models to improve pre-clinical studies.

Summary Statement

Exploring the tumour microenvironment in cholangiocarcinoma enables key pathways to be restored in pre-clinical models, enhancing their accuracy and application in understanding of cancer progression.

Introduction

Cholangiocarcinoma (CCA) is a highly malignant tumour arising from the biliary epithelium, characterised by its aggressive behaviour and poor prognosis (Razumilava and Gores, 2014). Traditional two-dimensional (2D) cell culture systems have been extensively used to study CCA, but they often fail to recapitulate the complex architecture and microenvironment of tumours, since they lack multi-dimensional cell-cell interactions and, usually, molecular and cellular stromal elements, resulting in limited translational relevance (Antoni *et al.*, 2015). In recent years, three-dimensional (3D) cell culture models, have emerged as valuable tools for investigating the biology and therapeutic responses of CCA (Mikhail, Eetezadi and Allen, 2013; Gilazieva *et al.*, 2020). However, while compared to traditional 2D models, 3D models, such as spheroids and organoids, better reflect the heterogeneity and complexity of solid tumours, making them more physiologically relevant for studying tumour behaviour and drug responses (Edmondson *et al.*, 2014; Vinci *et al.*, 2012), such models still lack stromal cells (Gilazieva *et al.*, 2020).

CCA is histologically characterised as a highly desmoplastic tumour. The abundant fibrotic stroma that surrounds and infiltrates the tumour is also known to modulate the progression and invasiveness of CCA (Fabris *et al.*, 2019; Sirica and Gores, 2014; Affo *et al.*, 2021). The CCA stroma consists of cancer-associated fibroblasts (CAFs), endothelial and lymphatic cells and a complex collection of inflammatory cells (macrophages, NK, neutrophils, and T cells) (Banales *et al.*, 2020). In addition to this, the tumour stroma also contains an extensive network of extracellular matrix (ECM) proteins (laminin, collagens, and fibronectin) (Govaere *et al.*, 2016; Szendroi and Lapis, 1985).

Studies have shown that CAFs can originate from bone marrow-derived circulating mesenchymal cells (Russo *et al.*, 2006), liver-resident hematopoietic stem cells (HSCs) (Okabe *et al.*, 2009) and/or portal fibroblasts (Dranoff and Wells, 2010). They are characterised by expression of several markers, the most common ones being α-SMA, the mucin-like transmembrane glycoprotein podoplanin, and the cell surface metalloprotease CD10. CAFs are the major component in the CCA tumour microenvironment (TME), and its

Disease Models & Mechanisms • DMM • Accepted manuscript

presence correlates to poor patient survival (Chuaysri *et al.*, 2009). CAFs, in the context of iCCA, are a hugely heterogeneous population displaying distinctive phenotypic traits (Fabris, Andersen and Fouassier, 2020; Affo *et al.*, 2021).

CAFs can shape the TME as well as influencing tumour growth and invasion through releasing pro-oncogenic paracrine mediators. These include TGF-β1, hepatocyte growth factor (HGF), EGF, SDF-1, connective tissue growth factor (CTGF), ECM components, and matrix metalloproteinases (MMPs) (Sirica, 2011). One of the most significant signalling pathways between CCA cells and CAFs is the HB-EGF/EGFR signalling pathway; in which there is an intense two-way communication by which CCA cells activate CAFs and in turn, CAFs sustain the invasive phenotype of cancer cells; activation of the receptor triggers TGF-β1 production by CCA cells, further enhancing fibroblast activation and CAF synthesis of HB-EGF (Claperon *et al.*, 2013).

When modelling cancer with an aim of understanding the underlying biology, identifying potential therapeutic targets and screening new therapeutic agents, molecular heterogeneity and the complexity of the stromal influence should be taken into consideration (Affo *et al.*, 2021; Song *et al.*, 2022; Zhang *et al.*, 2020). However, standard 2D models based on such cells are missing the influence of the TME and likely have adapted to growth on plastic in nutrient-rich conditions. Organoid models, although involving growth in a 3D setting directly from patient samples, lack other aspects of the TME, except where provided through use of complex media e.g. in the form of growth factors (van de Wetering *et al.*, 2015). Patient-derived xenograft (PDX) models, established by directly expanding patient tissue in an *in vivo* setting, theoretically maintain a more complex TME and provide a more clinically-relevant model (Hidalgo *et al.*, 2014). However, in common with other xenograft models, they are grown in immunodeficient mice and thus lack many of the TME's immune components (Kopetz, Lemos and Powis, 2012). Additionally, it has become apparent that the human stroma, transplanted along with the human cancer cells, is rapidly replaced by mouse stroma (Isella *et al.*, 2015; Jones *et al.*, 2023). Loss of human stromal cells in such models, potentially results in a disconnect where mouse-human interactions are not able to take place across the species barrier.

Therefore, this study aims firstly to identify signalling pathways that are lost in xenograft models in the absence of human stromal signalling and, secondly, to examine in CCA spheroid models derived from both cell lines and patient-derived xenografts, whether addition of mesenchymal stem cells (MSCs) can restore such pathways. MSCs have recently gained attention for their role in tumour growth and progression (Spaeth *et al.*, 2009; Pal *et al.*, 2020). They are multipotent stromal cells that are recruited by tumours and can be derived from various sources including bone marrow, adipose tissue, and umbilical cord

Disease Models & Mechanisms • DMM • Accepted manuscript

(Bieback and Brinkmann, 2010). These cells possess immunomodulatory properties and can interact with tumour cells, influencing many aspects of tumour biology, such as proliferation, angiogenesis, and the tumour microenvironment (Hoogduijn *et al.*, 2013). While the impact of MSCs on CCA remains largely unexplored, studies in other cancer types have demonstrated their pro-tumorigenic effects following activation to become CAFs (Kidd *et al.*, 2009; Katsuda *et al.*, 2013).

Findings from this study have potential to enhance our understanding of the tumour-stroma crosstalk in CCA and provide insights into the roles of mesenchymal cells in this disease. The identification of upregulated genes, enriched pathways, and phenotypic characteristics of the spheroids may contribute to the development of personalised treatment approaches for CCA patients.

Results

Identification of Lost Signalling Pathways in PDXs Models and Restoration via MSC Addition in CCA Spheroid Models

Whole genome expression profiling was used to compare the human transcriptome of a panel of 7 CCA PDXs with that of the patient samples from which they were derived. Analysis of expression of markers of a variety of stromal populations (CAFs, endothelial and immune cells) derived from single cell expression analysis of CCA tumours (Zhang *et al.*, 2020) showed that human stromal cells are lost in the PDXs (Figure 1A) with the majority of markers at lower levels in the PDXs than their respective patient samples. This extends to markers of CCA CAF subtypes (Affo *et al.*, 2021) which are also mainly absent in the PDXs (Figure 1B).

Since paracrine signalling from stromal cells is known to drive activation of specific pathways in cancer cells and given the potential for complete loss of some stromal cells in immunodeficient mouse models, and/or species disconnect even where human stromal cells are replaced by mouse stromal cells, the possibility that some cancer-associated pathways are dysregulated in the PDXs was investigated.

First, human genes differentially expressed in the patient samples and PDXs were identified; then, based on this gene set, the canonical pathways predicted to be differentially active in the patient and PDX samples were examined using Qiagen Ingenuity Pathway Analysis (IPA). A broad set of signalling pathways was apparently affected (Figure 1C), including pathways associated with cancer (Figure 1D and Table S1).

Using IPA's Upstream Regulator Analysis, a wide range of upstream regulators was identified, including growth factors, cytokines, kinases, and transcription regulators (Table

Disease Models & Mechanisms • DMM • Accepted manuscript

S2), predicted to be driving signalling pathways dysregulated in the PDXs. Considering kinases as druggable targets and the rising use of PDX models for evaluating kinase inhibitors as potential anti-cancer agents, kinase-associated pathways were the focal point in the next stage of the analysis.

Some of the pathways apparently active in the patient samples and not in the PDXs include stromal signalling pathways that are not truly absent (e.g. signalling pathways associated with innate immune cells or endothelial cells) but present as mouse genes derived from mouse stromal cells, not considered in our analysis of human gene expression. Thus, in order to identify paracrine signalling pathways dysregulated more specifically in the cancer cells within the PDXs, the focus was directed to a subset of kinases whose expression was maintained or apparently enriched in the PDXs (suggesting they are present in the human cancer cell compartment, rather than the mouse stromal compartment) but whose associated downstream pathway was predicted to be activated in the patient samples compared with the PDXs (based on activation z-score>2) i.e. inhibited in the PDXs, designated as inhibited cancer-associated kinases (ICAKs) (Table S3). Such a situation could arise because, although the kinase is present, upstream events that would normally activate them are missing, as would be the case if a paracrine signalling molecule were absent or unable to bind to its cognate receptor. Heatmaps of the downstream components of the pathways driven by the top 3 of these ICAKs confirm that signalling in these pathways is attenuated in the PDXs (Figure 2A). Loss of such signalling potentially affects cancer-associated functional characteristics such as proliferation, survival, adhesion, migration, survival and invasion (Figure 2B).

Based on the histology of the PDXs (Figure 3A) and Principal Component Analysis (Figure 3B), it was observed that the PDXs fall into two categories – well-differentiated (WD) PDXs (Figure 3Ai), with histology resembling those of the original patient tissues, and more poorly-differentiated (PD) tumours (Figure 3Aii). Since there was potential for these two categories of PDX to be driven by different signalling pathways, analysis of upstream regulators for each separately was additionally carried out and ICAKS identified (Table S4 and S5). Interestingly, while there are common ICAKs dysregulated in both the WD- and PD-PDXs, there are ICAKs uniquely dysregulated in each type of PDX (Figure 3C).

In order to investigate the potential for restoring such signalling pathways, 3D spheroid co-culture models were established involving addition of iMSCs to CCA cancer cells. The rationale for use of MSCs is that these multipotent cells have potential to become activated to cancer-associated fibroblasts and provide human paracrine signals to restore those lost in xenografts and in standard mono-culture models (Kidd *et al.*, 2009; Katsuda *et al.*, 2013).

Disease Models & Mechanisms • DMM • Accepted manuscript

Viability and Growth Dynamics of CCA Spheroids in Mono- and Co-Culture with iMSCs

Spheroids of three CCA cell lines, KKU-M055, KKU-M213 and RBE, were established as mono-cultures (CCA cells only) or as co-cultures with the addition of iMSCs at a 1:2 ratio (cancer cells:iMSCs). The morphology of the spheroids formed from different cell lines exhibited distinct characteristics (Figure 4). Upon initial seeding, individual cells were observed. However, after 3 days, spheroids were formed by all three cell lines. KKU-M055 formed loosely packed spheroids, and the addition of iMSCs resulted in the formation of more compact spheroids (Figure 4A). In contrast, KKU-M213 formed spherical spheroids with well-defined edges, and this morphology was further enhanced by the presence of iMSCs (Figure 4B). The RBE cell line produced the smallest spheroids which, in the absence of iMSCs became smaller over time (Figure 4C). To further support these observations, the area of the spheroids was measured from the brightfield images at each timepoint. For KKU-M055 and KKU-M213, there was an increase in the area of both mono- and co-cultures over time. However, the addition of iMSCs in the RBE-derived spheroids led to an increased area, maintained over time (Figure 4D), which may reflect improved cell viability or formation of looser spheroids.

Next, the viability of the spheroids was assessed. The live/dead staining results confirmed the overall viability of the cells (Figure 5A-C). In both mono- and co-culture spheroids of all cell lines, more than 95% of the cells were viable, except for the RBE cells (Figure 5C), where the co-cultures with iMSCs exhibited higher EthD-1 staining, indicating increased cell death, indicating that larger spheroids do not necessarily reflect higher cell viability.

However, since the live/dead staining measurements cannot differentiate between signals derived from cancer cells and iMSCs, a more direct approach was adopted to measure cell viability specifically in the cancer cells. Cancer cells were transduced with a lentivirus to introduce the firefly luciferase gene, resulting in only the cancer cells emitting light upon addition of the luciferase substrate. The emitted light intensity at each timepoint served as a reflection of the number of viable cancer cells present. Results from the luminescent assay revealed that the growth of KKU-M213 cells as spheroids was significantly dependent on the addition of iMSCs ($p=0.016$, $n=3$). Conversely, the growth of KKU-M055 cells was higher in mono-culture spheroids ($p=0.002$, $n=3$). Interestingly, while viability of cancer cells was maintained over time in the RBE co-culture spheroids, there was no significant difference in growth between mono- and co-culture spheroids (Figure 5D).

Disease Models & Mechanisms • DMM • Accepted manuscript

Morphological and Phenotypic Characterisation of Cholangiocarcinoma Spheroids in Mono- and Co-Culture with iMSCs

To examine the detailed morphology of the CCA spheroids, paraffin-embedded sections of microarrayed CCA mono- and iMSCs co-culture spheroids were subjected to H&E staining. Furthermore, IHC was employed to confirm the biliary phenotype of the cells within the spheroids using CK7 and CK19 as markers. Vimentin staining was used to localise the iMSCs, while Ki-67 staining was performed to assess proliferation. For the RBE cells, some staining for monoculture spheroids is missing due to the smaller size of the spheroids compared to the others, preventing a meaningful comparison between mono- and co-culture.

Interestingly, the presence of ductal-like structures, similar to those in CCA patient tumours, was observed within the spheroids, particularly for KKU-M213 and RBE models (Figure 6A). The biliary phenotype was confirmed by positive expression of CK7 and CK19, except for KKU-M055 (Figure 6B and C). In the case of KKU-M213, vimentin staining was detected in the co-culture derived from this cell line, while absent in the monoculture. Conversely, for KKU-M055, positive staining for vimentin was observed in both co-culture and monoculture (Figure 6D). In the monoculture spheroids, only a minor population of Ki-67-positive cells was evident. However, in the co-cultures, a larger number of brightly stained Ki-67-positive nuclei was detected. RBE cells were the exception, where no Ki-67 positive cells were observed (Figure 6E). Quantification further supported these findings (Figure 6F) suggesting that iMSCs may drive proliferation of the CCA cells.

Investigation of the Crosstalk and Proliferation Mechanism Induced by iMSCs in CCA Cells in Co-Culture

Based on RNAseq analysis, the top upregulated genes in the co-cultures compared with the monocultures, ranked by the absolute values of fold-change, were shown to be *FN1*, *SPARC*, several members of the COL family, *WNT5A1*, *POSTN* and *CHI3L1* (Figure 7A).

Additionally, KEGG pathway enrichment analysis was performed to identify the biological pathways that were enriched in the co-culture conditions. Among the upregulated pathways, ECM-receptor interaction (FDR=5.8e-04) emerged as the most significantly enriched pathway. Notably, the PI3K-Akt signalling pathway (FDR=5.8e-04) contained the highest number of upregulated genes among these pathways (Figure 7B).

Cox proportional regression analysis for multiple genes was performed using dataset GSE89749 (Jusakul *et al.*, 2017) with selection of the subset of samples from patients (n=31) with anatomic subtype, intrahepatic, and fluke status, positive, to match the

Disease Models & Mechanisms • DMM • Accepted manuscript

characteristics of KKU-M213. The relationship between expression of the genes differentially expressed in the co-culture model (Table S6) and overall survival was investigated and Kaplan-Meier plots drawn (Figure S1). The analysis showed that 8 genes among the differentially expressed genes in the co-cultures compared with the monoculture were significantly associated with overall survival (Bonferroni corrected p-value<0.05); for 6 of these (*ANGPTL4*, *C16ORF45*, *VSTM2L*, *SERPINE2*, *CAPRIN2* and *SPOCD1*) which were upregulated in the co-cultures, high expression was associated with poor survival (Table S7).

Such genes may be derived from the MSCs in the co-cultures or from the cancer cells. While important since they are present in-patient samples and suggest a microenvironment within the co-cultures which are closer to those present in the patient, further analysis to identify paracrine signals activated in the cancer cells within the co-cultures was carried out. Using a similar approach to that taken comparing when comparing patient and PDX samples, IPA analysis was carried out. A range of signalling pathways (Figure 8A), including cancer-associated pathways (Figure 8B) were shown to be altered in the co-cultures with most pathways being activated. Upstream Regulator Analysis was again used to identify kinases that were potential upstream regulators of the changes observed in the co-culture models and overlap with the ICAKs investigated. 16 of the ICAKs, identified when analysing the PDXs as a whole were activated in the MSC co-cultures (Table S8), suggesting that the MSCs have potential to activate paracrine signal pathways lost when human stromal cells are replaced by mouse stromal cells in xenografts. The potential for MSCs to restore signalling pathways specific to the two types of PDXs (Table S9 and S10) was also investigated. They are able to activate pathways driven by a number of ICAKs common to the two PDX types but also kinases which are specific to each type (Figure 8C).

Considering the varied effects observed from co-culture with MSCs in different CCA cells, including both inhibition and enhancement of proliferation, the effects of activating such kinases were investigated. Those inactive in WD-PDXs, and with potential to be restored by additional of MSCs, include kinases such as ERBB3, EGFR, ERBB2 and MET, whose activation is associated with growth promotion (Jin, 2020; Yoshikawa *et al.*, 2008; Dai *et al.*, 2012), with ERBB2 (HER2), EGFR and MET associated with the proliferative molecular sub-class of CCA (Sia *et al.*, 2013). In contrast, PD-PDXs kinases with potential to be restored by addition of MSCs include ACVR1C (ALK7), MAP3K14 and ROR1 which may be inhibitors of tumour growth (Li *et al.*, 2023; Allen *et al.*, 2017; Michael *et al.*, 2019) and JAK1 involved in the STAT3 signalling pathway characteristic of the inflammatory molecular sub-class of CCA (Sia *et al.*, 2013).

Disease Models & Mechanisms • DMM • Accepted manuscript

Thus, the ability of cells derived from both types of PDX to form spheroids and the influence of addition of MSCs on their viability and growth in 3D culture was investigated.

Assessment of iMSC Effects on CCA Growth in 3D Models Using Patient-Derived Xenografts

CCA cells derived from each of the PDXs were used to establish mono- and co-culture spheroid models. The ability of cells from the PDXs to form spheroids varied based on their histological group: WD-PDXs required iMSCs for supporting spheroid formation while PD-PDXs readily formed spheroids in both mono- and co-cultures. Monoculture CCA1 CCA7, and CCA11 (Figure S2) spheroids were easily disintegrated with pipetting but live/dead staining demonstrated good viability of cells within the loose clusters. In the co-culture setting, CCA1, CCA7, and CCA11 spheroids initially formed loose cell aggregates on day 0, which then transformed into compact spheroids by day 3, gradually expanding in size over time. The co-culture spheroids derived from these PDXs maintained their structural integrity, exhibited good viability based on live/dead staining and, when cell viability was quantified using PrestoBlue, there was higher cell viability than in the monoculture spheroids. In contrast, monoculture CCA2, CCA4, CCA5 and CCA6 PDXs (Figure S3) readily formed well-defined spheroids, which were viable based on live/dead staining, and whose volume and viability, quantified by PrestoBlue, increased over time. However, when co-cultured with iMSCs, although these PDXs also formed stable, viable spheroids that grew over time, their volume and viability was lower than that of the monoculture spheroids.

Discussion

The findings presented in this study highlight the heterogeneous role of mesenchymal cells within CCA tumours with potential to either enhance or inhibit CCA cancer cell growth. Furthermore, they offer insights into the intricate interplay between CCA cells and mesenchymal cells within a 3D spheroid culture system, demonstrating that addition of MSCs to such models can activate signalling pathways missing in patient xenografts due to loss of a human stromal microenvironment. Effects of co-culture were observed across models employing both primary CCA, expanded as PDXs, as well as established cell lines, with insights into mechanisms at the molecular level provided by transcriptomic analysis.

Bioinformatic analysis of paired patient and PDX samples was used to identify pathways that are dysregulated in the PDXs, including in cancer cells within the xenografts, likely due to the absence of human stromal components that provide paracrine signals. Interestingly, one

Disease Models & Mechanisms • DMM • Accepted manuscript

of the pathways dysregulated was MET, which, in spite of maintained expression in the PDX, was not active. This can be explained by the known low affinity of mouse HGF for the human MET receptor, compared to human HGF; the receptor being differently phosphorylated in response to mouse HGF leads to aberrant signal transduction and reduced activation of the pathway (Ikebuchi *et al.*, 2013). Other paracrine signals absent in the PDXs may be due to similar species disconnects. We further observed that the PDXs fall into two categories – PD and WD types and whilst dysregulated pathways are shared between them, there are also pathways unique to each type. The signals that drive such pathways in patient tumours could be derived from multiple components of the tumour microenvironment. However, given the importance of mesenchymal cells in CCA, we investigated the effect of introducing MSCs into 3D spheroid models of CCA.

Spheroid formation and morphology varied between different cell lines, different PDXs and also between mono- and co-culture spheroids. Some cancer cells appear to have an innate ability to form spheroids, while others (represented both amongst the cell lines and PDXs) formed spheroids more easily in the presence of iMSCs. Furthermore, in some cases, small compact spheroids are formed, which were lacking in distinct structures. In contrast, ductal-like structures were apparent in some spheroids and in the case of one of the cell lines, these were more prominent when iMSCs were incorporated. The increased compactness of spheroids and the presence of prominent ductal structures suggest changes in cell adhesion, cell-cell interactions, and extracellular matrix deposition (Cuiffo and Karnoub, 2012; Yuan *et al.*, 2023; Ghosh *et al.*, 2020). This aligns with the broader concept of crosstalk between cancer cells and the surrounding stroma, which is known to fuel tumour progression and orchestrate dynamic ECM remodelling (Poornima *et al.*, 2022; Ridge, Sullivan and Glynn, 2017), as well as the upregulated expression of genes associated with extracellular matrix and ECM-receptor interaction in co-culture conditions in this study.

In spite of such changes, and consistent with other studies (Liang *et al.*, 2021; Hass, 2020), proliferation of some cancer cells may not be enhanced by the presence of iMSCs and may even be inhibited. Such cancer cells may have acquired mutations that make them autonomous, for example with constitutively activated growth receptors (Du and Lovly, 2018) and thus do not require paracrine signals or may be unable to provide signals required by MSCs to differentiate into activated cancer-associated fibroblasts (Shamai *et al.*, 2019; Blache *et al.*, 2019; Wang *et al.*, 2021). The latter scenario is particularly interesting as it may be that additional stromal cell signals (e.g. from immune cells) are required in some cases (Kuzet and Gaggioli, 2016).

Our data suggest that paracrine signals provided by MSCs have potential to activate both pro- and anti-proliferative signalling pathways. Examples of pro-proliferative pathways

Disease Models & Mechanisms • DMM • Accepted manuscript

include those involving ERBB3, EGFR, ERBB2 and MET (Jin, 2020; Yoshikawa *et al.*, 2008; Dai *et al.*, 2012), which were shown to be inhibited in the WD-PDXs compared to patient tissues and activated in our MSC co-culture model; this potentially explains why additional of MSCs to these PDXs *ex vivo* enhanced spheroid formation and viability. Examples of potentially anti-proliferative pathways activated by paracrine signalling include those involving ACVR1C (ALK7), MAP3K14 and ROR1, linked to inhibition of cancer growth including in the context of CCA (Li *et al.*, 2023; Allen *et al.*, 2017; Michael *et al.*, 2019). These pathways were missing in the PD-PDXs and *ex vivo* co-culture with MSCs inhibited this type of PDX. Of course, other signalling pathway such as RET and HK2, identified to be missing in the PD-PDXs and capable of being activated in MSC co-cultures, can be pro-proliferative, so ultimately the phenotypic outcome will be dependent on the balance of the signals received by the cells and its particular molecular make-up. In this respect, it is interesting that our 2 groups of PDXs, which appear to respond differently to paracrine signals from MSCs, bear some relationship to the molecular subtypes of CCA previously described, ERBB2 (HER2), EGFR and MET being considered markers of the proliferative molecular sub-class of CCA and JAK1 which is part of the STAT3 signalling pathway associated with the inflammatory molecular sub-class of CCA (Sia *et al.*, 2013). In the future it would be of interest to investigate associations with other molecular markers linked to poor therapeutic responses and outcomes which include mutations in drivers of proliferative signalling pathways such as KRAS, SMAD4 and FGFR2 and EPHA2 which may provide means for cancer cells to become independent of paracrine signalling (Wang *et al.*, 2022; Boerner *et al.*, 2021).

Our Kaplan-Meier analysis, which investigated the correlation between differentially expressed genes in the co-culture model and the overall survival of individuals with intrahepatic cholangiocarcinoma, provides support for the potential clinical relevance of the developed models. *ANGPTL4*, *C16ORF45*, *VSTM2L*, *SERPINE2*, *CAPRIN2* and *SPOCD1* emerged as key players significantly linked to overall survival, with elevated expression levels of these genes notably associated with unfavourable outcomes. While additional investigation is necessary to understand for example whether they are expressed in the cancer cells or in the stromal cells, our analysis demonstrates that expression levels are dependent on co-culture and provides insights into specific genes, such as *SERPINE2*, known for its involvement in extracellular matrix dynamics. In pancreatic cancer, *SERPINE2* overexpression has been associated with significantly increased local invasiveness, accompanied by a substantial increase in ECM production (Buchholz *et al.*, 2003). Furthermore, the observed association of *CAPRIN2* with cell cycle processes suggests a potential impact on cancer cell proliferation (Ai *et al.*, 2020). Understanding the role of these

Disease Models & Mechanisms • DMM • Accepted manuscript

genes can contribute to explaining the results of our models and establishing connections with clinical data.

Thus, this 3D co-culture model system provides potential for further investigation of these phenomena, including through more detailed analysis of signalling pathways activated in individual cells and PDXs, as well as building the complexity by addition of further cell-types.

Characterisation of models is crucial if they are to be effectively used in drug development. It is important not only to use models that represent the spectrum of molecular changes that occur in the cancer cells themselves but also to incorporate relevant aspects of the tumour microenvironment. In the absence of paracrine signals from stromal cells, pathways that are active in patients may be missed when searching for relevant drug targets, or potentially useful drugs might be discarded because the relevant pathway is missing in the model. The co-culture system described in this paper could serve as an invaluable platform for further interrogating the complex signalling mechanisms orchestrating tumour-stroma interactions, and for use in drug development.

Material and Methods

Cell Culture Conditions

Wildtype KKU-M055, KKU-M213, and RBE cell lines were obtained from Professor John Gordan at the University of California under a Material Transfer Agreement and subjected to STR profiling. Immortalised bone marrow-derived mesenchymal stem cells (iMSCs) were obtained through a collaboration with Dr. James Dixon from the School of Pharmacy at the University of Nottingham; they were immortalised by overexpression of TERT (Matta *et al.*, 2019). The CCA cell lines and iMSCs were cultured in high-glucose Dulbecco's Modified Essential Medium (DMEM) supplemented with 1 mM L-glutamine and 10% heat-inactivated fetal bovine serum (FBS) (10% DMEM) and were used below passage 40. All cell lines were incubated in a 5% CO_2 air-humidified atmosphere at 37°C. Regular mycoplasma tests were conducted monthly to confirm the absence of contamination in the cell cultures. Luminescent cell lines were created by lentiviral transduction of CCA cells with a pLVX-Puro Vector containing Firefly luciferase and a Puromycin resistance gene (Clontech, Takara Bio Company, Otsu, Japan).

Establishment of Spheroid Cultures

Cells were detached and resuspended in 10 mL of pre-warmed 10% DMEM. A concentration of 5000 cells/mL was added as a mono- or co-culture to each well in a 96-well ultra-low

Disease Models & Mechanisms • DMM • Accepted manuscript

attachment (ULA) round-bottom plate (Sigma #CLS3474). For the co-culture, cancer cells were co-cultured with iMSCs at a 1:2 ratio (cancer cells:MSCs). Mouse-derived basement membrane extract (BME) from Cultrex PathClear (Bio-techne, #3432-005-01) was thawed overnight on ice at 4°C and added at a concentration of 100 µg/mL. A volume of 200 µL (equivalent to 1000 cells) was added. The plate was centrifuged at 300g for 10 minutes and then incubated in a 5% CO_2 air-humidified atmosphere at 37°C.

Patient-Derived Xenograft Spheroids

Tumours (CCA1, CCA2, CCA4, CCA5, CCA6, CCA7, and CCA11) were obtained as fresh surgical material from tumour resections at Nottingham University Hospitals NHS Trust, collected with informed patient consent and National Research Ethics Service (NRES) approval (NRES REC 10/H0405/6) and used in accordance with NRES approval (NRES REC 08/H0403/37). Immunodeficient female $Rag2^{-/-}$ $\gamma C^{-/-}$ (Rag2G, 8–10 weeks) bred in-house under Home Office Project Licence P375A76F were used in this project; as only small numbers of mice were required for each initiation, we used what was available from our small in-house colony, which happened to be females, rather than custom breed mixed cohorts for this project, generating excess animals in the process. PDXs were generated by implantation of minced tumour fragments admixed with Matrigel (BD Biosciences) using an implant trochar (VetTech, UK) subcutaneously under local anaesthetic (EMLA Cream, Aspen Pharma, Ireland) in the mice under HO project license 3003444, having been approved by the University of Nottingham AWERB. Mice were maintained in individually ventilated cages (IVCs) (Tecniplast UK) within a barriered unit illuminated by fluorescent lights set to give a 12-hour light-dark cycle, as recommended in the United Kingdom Home Office Animals (Scientific Procedures) Act 1986. The room was air-conditioned by a system designed to maintain an air temperature range of 21 ± 2 °C and a humidity of 55% + 10%. Mice were housed in social groups during the procedure and provided with irradiated bedding and autoclaved nesting materials and environmental enrichment (Datesand, UK). Sterile irradiated 5V5R rodent diet (IPS Ltd, UK) and irradiated water (SLS, UK) was offered *ad libitum*. NCRI guidelines for the welfare and use of animals in cancer research, LASA good practice guidelines and FELASA working group on pain and distress guidelines were also followed, as were the ARRIVE guidelines on the reporting of in vivo experiments. Tumours were measured weekly using Vernier calipers, and the volumes were calculated using the formula V = ab2/6, where a is the length and b is the width. Mice were also weighed weekly and given a daily health check by an experienced technician. Upon reaching maximum growth as allowed under the NCRI guidelines (mean diameter 1.2cm), mice were killed by a Schedule 1 method (cervical dislocation), tumours were removed under aseptic conditions

Disease Models & Mechanisms • DMM • Accepted manuscript

and, during PDX passage, tissue was obtained, and cells isolated for use in spheroid models, using protocols previously established in our laboratory (Onion *et al.*, 2016).

The cells were manually counted using a Neubauer chamber, and 1000 CCA cells were seeded for the spheroid monoculture. For the spheroid co-culture, CCA cells were mixed with iMSCs at a 1:2 ratio (cancer cells:iMSCs). The cells, either alone or mixed, were seeded in ULA 96-well plates at a total volume of 200 µL per well. BME was added at a final concentration of 300 µg/mL. After centrifugation at 300g for 10 minutes, the plates were placed in an incubator, maintaining a 5% CO_2 air-humidified atmosphere at 37°C.

Live/Dead Cell Staining in Spheroid Culture

Live/dead staining was performed using a commercially available and pre-optimised kit. Spheroids were washed with pre-warmed PBS and incubated with a solution containing 40 µM of Ethidium homodimer (EthD-1) and 20 µM of Calcein Acetoxymethyl Ester (Ca-AM). Cell imaging was performed using a fluorescence microscope.

Viability Assays

Viability assays were conducted using PrestoBlue and the luciferase assay. For PrestoBlue assay, 100µL of high-glucose DMEM was removed from each well and 10 µL of PrestoBlue was added in each well. After incubation, the absorbance was measured using a microplate reader. For the luciferase assay, 10 µL of D-Luciferin (30mg/mL) was added to each well and the bioluminescence signal was measured using a luminometer reader.

Histology

The spheroids were washed three times with PBS and fixed overnight at 4°C in 4% paraformaldehyde (PFA). After two further PBS washes, they were embedded in 2% agarose, fixed in 1× Neutral buffer formalin (NBF), and paraffin embedded to prepare spheroid microarrays according to the published protocol (Ivanov & Grabowska, 2017). For further characterisation of the spheroids, paraffin-embedded sections were prepared. Hematoxylin and eosin (H&E) staining was performed to examine the morphology and internal structures of the spheroids. Immunohistochemistry staining was conducted to confirm the biliary phenotype using CK7 (Dako, #M7018) and CK19 (Dako, #M0888) as markers. Vimentin (Dako, #M0725) staining was employed to localise iMSCs within the co-culture spheroids. Ki-67 (Dako, #M7240) staining was performed to assess cell proliferation.

Disease Models & Mechanisms • DMM • Accepted manuscript

Positive expression was quantified in 5 areas of each section by manually counting the positive cells and cancer cells and calculating the ratio of positively stained cancer cells over the total of cancer cells observed in each area.

RNASeq

RNA extraction was performed following the AllPrep DNA/RNA/Protein SOP (Qiagen #80004). Subsequently, RNA sequencing was carried out by Novogene (Cambridge, UK). The sequencing data underwent quality trimming and genome alignment (GRCh38). Integrated Differential Expression and Pathway analysis (iDEP) was used to generate an expression matrix, filter the data, and convert it to Ensemble gene IDs. Differential expression analysis was conducted using the DESeq2 package. JVolcano plots were employed to visualise gene expression patterns. Pathway analysis was conducted using Gene Set Enrichment Analysis (GSEA), using fold-change values obtained from DESeq2 results. The most significant hallmarks were selected and represented as KEGG-enrichment plots. Data were also analysed through the use of QIAGEN Ingenuity Pathway Analysis (QIAGEN Inc., https://digitalinsights.qiagen.com/IPA), in particular the canonical pathways and upstream regulator modules (Krämer *et al.*, 2013). Canonical pathways analysis identified the pathways from the QIAGEN Ingenuity Pathway Analysis library of canonical pathways that were most significantly dysregulated and Upstream Regulator analysis identified upstream molecules predicted to be driving these changes. The significance of the association between the data set and the canonical pathway/upstream regulator was measured by calculating a p-value determining the probability that the association between the genes in the dataset and the canonical pathway is explained by chance alone and by calculation of a z-score to indicate the likelihood of activation or inhibition of that pathway. A z-score of greater or less than 2 was considered significant. Heatmaps were drawn using Morpheus (https://software.broadinstitute.org/morpheus/) and Venn diagrams using Venny (https://bioinfogp.cnb.csic.es/tools/venny/).

Image Analysis

The ImageJ software was applied to measure the area of spheroids by using a plugin application of ImageJ.

Disease Models & Mechanisms • DMM • Accepted manuscript

Analysis

Statistical analysis was performed using GraphPad Prism Version 9.4.1. For the 3D luciferase assays, the difference in cell viability between monoculture and different co-cultures on each individual day was analysed using paired t-tests. Error bars were represented as mean ± standard error of the mean (SEM). A significance level of $p<0.05$ was considered statistically significant. Cox proportional regression analysis for multiple genes and Kaplan-Meier analysis were carried out using the R2 Genomics Analysis and Visualization Platform (http://r2.amc.nl) and statistical significance was tested using the log-rank test with Bonferroni correction to allow for multiple testing.

Acknowledgements

We are grateful to Dr James Dixon (University of Nottingham) for access to his immortalised MSCs.

Competing interests

We are not aware of any competing interests.

Funding

This project was supported by a PhD studentship (for MSC) and a Strategic Funding Award (to AMG) and Anne McLaren Fellowship (to JCA) from University of Nottingham.

Data availability

N/A

Author contributions statement

Conceptualization: M.S.C., J.B.A., D.O.B., A.M.G.; Methodology: M.S.C., A.M.G., P.C., C.P., A.R., M.M.; Validation: M.S.C.; Formal analysis: M.S.C., E.C.R., J.C.A., N.P.M, A.M.G.; Investigation: M.S.C, P.C., C.P., A.R., M.M.; Resources: P.C., C.P., A.R., M.M.; Data

Disease Models & Mechanisms • DMM • Accepted manuscript

curation: M.S.C., E.C.R., J.C.A., N.P.M., A.M.G.; Writing - original draft: M.S.C.; Writing - review & editing: M.S.C., E.C.R., J.C.A., P.C., C.P., A.R., M.M., N.P.M., I.U.E., J.B.A., D.O.B., A.M.G.; Visualization: M.S.C., J.C.A., A.M.G.; Supervision: D.O.B., A.M.G.; Project administration: M.S.C.

Diversity and inclusion statement

N/A

References

Affo, S., Nair, A., Brundu, F., Ravichandra, A., Bhattacharjee, S., Matsuda, M., Chin, L., Filliol, A., Wen, W., Song, X., Decker, A., Worley, J., Caviglia, J. M., Yu, L., Yin, D., Saito, Y., Savage, T., Wells, R. G., Mack, M., Zender, L., Arpaia, N., Remotti, H. E., Rabadan, R., Sims, P., Leblond, A. L., Weber, A., Riener, M. O., Stockwell, B. R., Gaublomme, J., Llovet, J. M., Kalluri, R., Michalopoulos, G. K., Seki, E., Sia, D., Chen, X., Califano, A. and Schwabe, R. F. (2021) 'Promotion of cholangiocarcinoma growth by diverse cancer-associated fibroblast subpopulations', *Cancer Cell,* 39(6), pp. 866-882.e11.

Ai, Y., Wu, S., Zou, C. and Wei, H. (2020) 'LINC00941 promotes oral squamous cell carcinoma progression via activating CAPRIN2 and canonical WNT/β-catenin signaling pathway', *J Cell Mol Med,* 24(18), pp. 10512-10524.

Allen, I. C., Eden, K., Heid, B. and Holl, E. K. (2017) 'Map3K14 signaling attenuates the development of colorectal cancer through activation of the non-canonical NF-κB signaling cascade', *The Journal of Immunology,* 198(1_Supplement), pp. 197.6-197.6.

Antoni, D., Burckel, H., Josset, E. and Noel, G. (2015) 'Three-dimensional cell culture: a breakthrough in vivo', *Int J Mol Sci,* 16(3), pp. 5517-27.

Banales, J. M., Marin, J. J. G., Lamarca, A., Rodrigues, P. M., Khan, S. A., Roberts, L. R., Cardinale, V., Carpino, G., Andersen, J. B., Braconi, C., Calvisi, D. F., Perugorria, M. J., Fabris, L., Boulter, L., Macias, R. I. R., Gaudio, E., Alvaro, D., Gradilone, S. A., Strazzabosco, M., Marzioni, M., Coulouarn, C., Fouassier, L., Raggi, C., Invernizzi, P., Mertens, J. C., Moncsek, A., Rizvi, S., Heimbach, J., Koerkamp, B. G., Bruix, J., Forner, A., Bridgewater, J., Valle, J. W. and Gores, G. J. (2020) 'Cholangiocarcinoma 2020: the next horizon in mechanisms and management', *Nat Rev Gastroenterol Hepatol,* 17(9), pp. 557-588.

Bieback, K. and Brinkmann, I. (2010) 'Mesenchymal stromal cells from human perinatal tissues: From biology to cell therapy', *World J Stem Cells,* 2(4), pp. 81-92.

Disease Models & Mechanisms • DMM • Accepted manuscript

Blache, U., Horton, E. R., Xia, T., Schoof, E. M., Blicher, L. H., Schonenberger, A., Snedeker, J. G., Martin, I., Erler, J. T. and Ehrbar, M. (2019) 'Mesenchymal stromal cell activation by breast cancer secretomes in bioengineered 3D microenvironments', *Life Sci Alliance,* 2(3).

Boerner, T., Drill, E., Pak, L. M., Nguyen, B., Sigel, C. S., Doussot, A., Shin, P., Goldman, D. A., Gonen, M., Allen, P. J., Balachandran, V. P., Cercek, A., Harding, J., Solit, D. B., Schultz, N., Kundra, R., Walch, H., D'Angelica, M. I., DeMatteo, R. P., Drebin, J., Kemeny, N. E., Kingham, T. P., Simpson, A. L., Hechtman, J. F., Vakiani, E., Lowery, M. A., Ijzermans, J. N. M., Buettner, S., Koerkamp, B. G., Doukas, M., Chandwani, R. and Jarnagin, W. R. (2021) 'Genetic Determinants of Outcome in Intrahepatic Cholangiocarcinoma', *Hepatology,* 74(3), pp. 1429-1444.

Buchholz, M., Biebl, A., Neesse, A., Wagner, M., Iwamura, T., Leder, G., Adler, G. and Gress, T. M. (2003) 'SERPINE2 (protease nexin I) promotes extracellular matrix production and local invasion of pancreatic tumors in vivo', *Cancer Res,* 63(16), pp. 4945-51.

Chuaysri, C., Thuwajit, P., Paupairoj, A., Chau-In, S., Suthiphongchai, T. and Thuwajit, C. (2009) 'Alpha-smooth muscle actin-positive fibroblasts promote biliary cell proliferation and correlate with poor survival in cholangiocarcinoma', *Oncol Rep,* 21(4), pp. 957-69.

Claperon, A., Mergey, M., Aoudjehane, L., Ho-Bouldoires, T. H., Wendum, D., Prignon, A., Merabtene, F., Firrincieli, D., Desbois-Mouthon, C., Scatton, O., Conti, F., Housset, C. and Fouassier, L. (2013) 'Hepatic myofibroblasts promote the progression of human cholangiocarcinoma through activation of epidermal growth factor receptor', *Hepatology,* 58(6), pp. 2001-11.

Cuiffo, B. G. and Karnoub, A. E. (2012) 'Mesenchymal stem cells in tumor development: emerging roles and concepts', *Cell Adh Migr,* 6(3), pp. 220-30.

Dai, R., Li, J., Fu, J., Chen, Y., Wang, R., Zhao, X., Luo, T., Zhu, J., Ren, Y., Cao, J., Qian, Y., Li, N. and Wang, H. (2012) 'The Tyrosine Kinase c-Met Contributes to the Pro-tumorigenic Function of the p38 Kinase in Human Bile Duct Cholangiocarcinoma Cells*', *Journal of Biological Chemistry,* 287(47), pp. 39812-39823.

Dranoff, J. A. and Wells, R. G. (2010) 'Portal fibroblasts: Underappreciated mediators of biliary fibrosis', *Hepatology,* 51(4), pp. 1438-44.

Du, Z. and Lovly, C. M. (2018) 'Mechanisms of receptor tyrosine kinase activation in cancer', *Mol Cancer,* 17(1), pp. 58.

Edmondson, R., Broglie, J. J., Adcock, A. F. and Yang, L. (2014) 'Three-dimensional cell culture systems and their applications in drug discovery and cell-based biosensors', *Assay Drug Dev Technol,* 12(4), pp. 207-18.

Disease Models & Mechanisms • DMM • Accepted manuscript

Fabris, L., Andersen, J. B. and Fouassier, L. (2020) 'Intrahepatic cholangiocarcinoma: A single-cell resolution unraveling the complexity of the tumor microenvironment', *J Hepatol,* 73(5), pp. 1007-1009.

Fabris, L., Perugorria, M. J., Mertens, J., Bjorkstrom, N. K., Cramer, T., Lleo, A., Solinas, A., Sanger, H., Lukacs-Kornek, V., Moncsek, A., Siebenhuner, A. and Strazzabosco, M. (2019) 'The tumour microenvironment and immune milieu of cholangiocarcinoma', *Liver Int,* 39 Suppl 1, pp. 63-78.

Ghosh, D., Mejia Pena, C., Quach, N., Xuan, B., Lee, A. H. and Dawson, M. R. (2020) 'Senescent mesenchymal stem cells remodel extracellular matrix driving breast cancer cells to a more-invasive phenotype', *J Cell Sci,* 133(2).

Gilazieva, Z., Ponomarev, A., Rutland, C., Rizvanov, A. and Solovyeva, V. (2020) 'Promising Applications of Tumor Spheroids and Organoids for Personalized Medicine', *Cancers (Basel),* 12(10).

Govaere, O., Wouters, J., Petz, M., Vandewynckel, Y. P., Van den Eynde, K., Van den Broeck, A., Verhulst, S., Dollé, L., Gremeaux, L., Ceulemans, A., Nevens, F., van Grunsven, L. A., Topal, B., Vankelecom, H., Giannelli, G., Van Vlierberghe, H., Mikulits, W., Komuta, M. and Roskams, T. (2016) 'Laminin-332 sustains chemoresistance and quiescence as part of the human hepatic cancer stem cell niche', *J Hepatol,* 64(3), pp. 609-17.

Hass, R. (2020) 'Role of MSC in the Tumor Microenvironment', *Cancers (Basel),* 12(8).

Hidalgo, M., Amant, F., Biankin, A. V., Budinska, E., Byrne, A. T., Caldas, C., Clarke, R. B., de Jong, S., Jonkers, J., Maelandsmo, G. M., Roman-Roman, S., Seoane, J., Trusolino, L. and Villanueva, A. (2014) 'Patient-derived xenograft models: an emerging platform for translational cancer research', *Cancer Discov,* 4(9), pp. 998-1013.

Hoogduijn, M. J., Roemeling-van Rhijn, M., Engela, A. U., Korevaar, S. S., Mensah, F. K., Franquesa, M., de Bruin, R. W., Betjes, M. G., Weimar, W. and Baan, C. C. (2013) 'Mesenchymal stem cells induce an inflammatory response after intravenous infusion', *Stem Cells Dev,* 22(21), pp. 2825-35.

Ikebuchi, F., Oka, K., Mizuno, S., Fukuta, K., Hayata, D., Ohnishi, H. and Nakamura, T. (2013) 'Dissociation of c-Met phosphotyrosine sites in human cells in response to mouse hepatocyte growth factor but not human hepatocyte growth factor: the possible roles of different amino acids in different species', *Cell Biochem Funct,* 31(4), pp. 298-304.

Isella, C., Terrasi, A., Bellomo, S. E., Petti, C., Galatola, G., Muratore, A., Mellano, A., Senetta, R., Cassenti, A., Sonetto, C., Inghirami, G., Trusolino, L., Fekete, Z., De Ridder, M., Cassoni, P., Storme, G., Bertotti, A. and Medico, E. (2015) 'Stromal contribution to the colorectal cancer transcriptome', *Nat Genet,* 47(4), pp. 312-319.

Jin, W. (2020) 'ErBb Family Proteins in Cholangiocarcinoma and Clinical Implications', *J Clin Med,* 9(7).

Disease Models & Mechanisms • DMM • Accepted manuscript

Jones, S., Ashworth, J. C., Meakin, M., Collier, P., Probert, C., Ritchie, A. A., Merry, C. L. R. and Grabowska, A. M. (2023) 'Application of a 3D hydrogel-based model to replace use of animals for passaging patient-derived xenografts', *In Vitro Model,* 2(3-4), pp. 99-111.

Jusakul, A., Cutcutache, I., Yong, C. H., Lim, J. Q., Huang, M. N., Padmanabhan, N., Nellore, V., Kongpetch, S., Ng, A. W. T., Ng, L. M., Choo, S. P., Myint, S. S., Thanan, R., Nagarajan, S., Lim, W. K., Ng, C. C. Y., Boot, A., Liu, M., Ong, C. K., Rajasegaran, V., Lie, S., Lim, A. S. T., Lim, T. H., Tan, J., Loh, J. L., McPherson, J. R., Khuntikeo, N., Bhudhisawasdi, V., Yongvanit, P., Wongkham, S., Totoki, Y., Nakamura, H., Arai, Y., Yamasaki, S., Chow, P. K., Chung, A. Y. F., Ooi, L., Lim, K. H., Dima, S., Duda, D. G., Popescu, I., Broet, P., Hsieh, S. Y., Yu, M. C., Scarpa, A., Lai, J., Luo, D. X., Carvalho, A. L., Vettore, A. L., Rhee, H., Park, Y. N., Alexandrov, L. B., Gordân, R., Rozen, S. G., Shibata, T., Pairojkul, C., Teh, B. T. and Tan, P. (2017) 'Whole-Genome and Epigenomic Landscapes of Etiologically Distinct Subtypes of Cholangiocarcinoma', *Cancer Discov,* 7(10), pp. 1116-1135.

Katsuda, T., Tsuchiya, R., Kosaka, N., Yoshioka, Y., Takagaki, K., Oki, K., Takeshita, F., Sakai, Y., Kuroda, M. and Ochiya, T. (2013) 'Human adipose tissue-derived mesenchymal stem cells secrete functional neprilysin-bound exosomes', *Sci Rep,* 3, pp. 1197.

Kidd, S., Spaeth, E., Dembinski, J. L., Dietrich, M., Watson, K., Klopp, A., Battula, V. L., Weil, M., Andreeff, M. and Marini, F. C. (2009) 'Direct evidence of mesenchymal stem cell tropism for tumor and wounding microenvironments using in vivo bioluminescent imaging', *Stem Cells,* 27(10), pp. 2614-23.

Kopetz, S., Lemos, R. and Powis, G. (2012) 'The Promise of Patient-Derived Xenografts: The Best Laid Plans of Mice and Men', *Clinical Cancer Research,* 18(19), pp. 5160-5162.

Krämer, A., Green, J., Pollard, J., Jr and Tugendreich, S. (2013) 'Causal analysis approaches in Ingenuity Pathway Analysis', *Bioinformatics,* 30(4), pp. 523-530.

Kuzet, S. E. and Gaggioli, C. (2016) 'Fibroblast activation in cancer: when seed fertilizes soil', *Cell Tissue Res,* 365(3), pp. 607-19.

Li, X., Sun, Z., Wang, L., Wang, Q., Wang, M., Guo, J., Li, H., Chen, M., Cao, G., Yu, Y., Zhong, H., Zou, H., Ma, K., Zhang, B., Wang, G. and Feng, Y. (2023) 'ROR1-AS1 might promote in vivo and in vitro proliferation and invasion of cholangiocarcinoma cells', *BMC Cancer,* 23(1), pp. 912.

Liang, W., Chen, X., Zhang, S., Fang, J., Chen, M., Xu, Y. and Chen, X. (2021) 'Mesenchymal stem cells as a double-edged sword in tumor growth: focusing on MSC-derived cytokines', *Cell Mol Biol Lett,* 26(1), pp. 3.

Matta, C., Boocock, D. J., Fellows, C. R., Miosge, N., Dixon, J. E., Liddell, S., Smith, J. and Mobasheri, A. (2019) 'Molecular phenotyping of the surfaceome of migratory

Disease Models & Mechanisms • DMM • Accepted manuscript

chondroprogenitors and mesenchymal stem cells using biotinylation, glycocapture and quantitative LC-MS/MS proteomic analysis', *Scientific Reports,* 9(1), pp. 9018.

Michael, I. P., Saghafinia, S., Tichet, M., Zangger, N., Marinoni, I., Perren, A. and Hanahan, D. (2019) 'ALK7 Signaling Manifests a Homeostatic Tissue Barrier That Is Abrogated during Tumorigenesis and Metastasis', *Dev Cell,* 49(3), pp. 409-424.e6.

Mikhail, A. S., Eetezadi, S. and Allen, C. (2013) 'Multicellular tumor spheroids for evaluation of cytotoxicity and tumor growth inhibitory effects of nanomedicines in vitro: a comparison of docetaxel-loaded block copolymer micelles and Taxotere(R)', *PLoS One,* 8(4), pp. e62630.

Okabe, H., Beppu, T., Hayashi, H., Horino, K., Masuda, T., Komori, H., Ishikawa, S., Watanabe, M., Takamori, H., Iyama, K. and Baba, H. (2009) 'Hepatic stellate cells may relate to progression of intrahepatic cholangiocarcinoma', *Ann Surg Oncol,* 16(9), pp. 2555-64.

Onion, D., Argent, R. H., Reece-Smith, A. M., Craze, M. L., Pineda, R. G., Clarke, P. A., Ratan, H. L., Parsons, S. L., Lobo, D. N., Duffy, J. P., Atherton, J. C., McKenzie, A. J., Kumari, R., King, P., Hall, B. M. and Grabowska, A. M. (2016) '3-Dimensional Patient-Derived Lung Cancer Assays Reveal Resistance to Standards-of-Care Promoted by Stromal Cells but Sensitivity to Histone Deacetylase Inhibitors', *Mol Cancer Ther,* 15(4), pp. 753-63.

Pal, A., Ashworth, J. C., Collier, P., Probert, C., Jones, S., Leza, E. P., Meakin, M. L., A, A. R., Onion, D., Clarke, P. A., Allegrucci, C. and Grabowska, A. M. (2020) 'A 3D Heterotypic Breast Cancer Model Demonstrates a Role for Mesenchymal Stem Cells in Driving a Proliferative and Invasive Phenotype', *Cancers (Basel),* 12(8).

Poornima, K., Francis, A. P., Hoda, M., Eladl, M. A., Subramanian, S., Veeraraghavan, V. P., El-Sherbiny, M., Asseri, S. M., Hussamuldin, A. B. A., Surapaneni, K. M., Mony, U. and Rajagopalan, R. (2022) 'Implications of Three-Dimensional Cell Culture in Cancer Therapeutic Research', *Front Oncol,* 12, pp. 891673.

Razumilava, N. and Gores, G. J. (2014) 'Cholangiocarcinoma', *Lancet,* 383(9935), pp. 2168-79.

Ridge, S. M., Sullivan, F. J. and Glynn, S. A. (2017) 'Mesenchymal stem cells: key players in cancer progression', *Mol Cancer,* 16(1), pp. 31.

Russo, F. P., Alison, M. R., Bigger, B. W., Amofah, E., Florou, A., Amin, F., Bou-Gharios, G., Jeffery, R., Iredale, J. P. and Forbes, S. J. (2006) 'The bone marrow functionally contributes to liver fibrosis', *Gastroenterology,* 130(6), pp. 1807-21.

Shamai, Y., Alperovich, D. C., Yakhini, Z., Skorecki, K. and Tzukerman, M. (2019) 'Reciprocal Reprogramming of Cancer Cells and Associated Mesenchymal Stem Cells in Gastric Cancer', *Stem Cells,* 37(2), pp. 176-189.

Sia, D., Hoshida, Y., Villanueva, A., Roayaie, S., Ferrer, J., Tabak, B., Peix, J., Sole, M., Tovar, V., Alsinet, C., Cornella, H., Klotzle, B., Fan, J. B., Cotsoglou, C., Thung, S. N.,

Disease Models & Mechanisms • DMM • Accepted manuscript

Fuster, J., Waxman, S., Garcia-Valdecasas, J. C., Bruix, J., Schwartz, M. E., Beroukhim, R., Mazzaferro, V. and Llovet, J. M. (2013) 'Integrative molecular analysis of intrahepatic cholangiocarcinoma reveals 2 classes that have different outcomes', *Gastroenterology,* 144(4), pp. 829-40.

Sirica, A. E. (2011) 'The role of cancer-associated myofibroblasts in intrahepatic cholangiocarcinoma', *Nat Rev Gastroenterol Hepatol,* 9(1), pp. 44-54.

Sirica, A. E. and Gores, G. J. (2014) 'Desmoplastic stroma and cholangiocarcinoma: clinical implications and therapeutic targeting', *Hepatology,* 59(6), pp. 2397-402.

Song, G., Shi, Y., Meng, L., Ma, J., Huang, S., Zhang, J., Wu, Y., Li, J., Lin, Y., Yang, S., Rao, D., Cheng, Y., Lin, J., Ji, S., Liu, Y., Jiang, S., Wang, X., Zhang, S., Ke, A., Wang, X., Cao, Y., Ji, Y., Zhou, J., Fan, J., Zhang, X., Xi, R. and Gao, Q. (2022) 'Single-cell transcriptomic analysis suggests two molecularly distinct subtypes of intrahepatic cholangiocarcinoma', *Nature Communications,* 13(1), pp. 1642.

Spaeth, E. L., Dembinski, J. L., Sasser, A. K., Watson, K., Klopp, A., Hall, B., Andreeff, M. and Marini, F. (2009) 'Mesenchymal stem cell transition to tumor-associated fibroblasts contributes to fibrovascular network expansion and tumor progression', *PLoS ONE,* 4(4), pp. e4992.

Szendroi, M. and Lapis, K. (1985) 'Distribution of fibronectin and laminin in human liver tumors', *J Cancer Res Clin Oncol,* 109(1), pp. 60-4.

van de Wetering, M., Francies, H. E., Francis, J. M., Bounova, G., Iorio, F., Pronk, A., van Houdt, W., van Gorp, J., Taylor-Weiner, A., Kester, L., McLaren-Douglas, A., Blokker, J., Jaksani, S., Bartfeld, S., Volckman, R., van Sluis, P., Li, V. S., Seepo, S., Sekhar Pedamallu, C., Cibulskis, K., Carter, S. L., McKenna, A., Lawrence, M. S., Lichtenstein, L., Stewart, C., Koster, J., Versteeg, R., van Oudenaarden, A., Saez-Rodriguez, J., Vries, R. G., Getz, G., Wessels, L., Stratton, M. R., McDermott, U., Meyerson, M., Garnett, M. J. and Clevers, H. (2015) 'Prospective derivation of a living organoid biobank of colorectal cancer patients', *Cell,* 161(4), pp. 933-45.

Vinci, M., Gowan, S., Boxall, F., Patterson, L., Zimmermann, M., Court, W., Lomas, C., Mendiola, M., Hardisson, D. and Eccles, S. A. (2012) 'Advances in establishment and analysis of three-dimensional tumor spheroid-based functional assays for target validation and drug evaluation', *BMC Biol,* 10, pp. 29.

Wang, M., Zhao, X., Qiu, R., Gong, Z., Huang, F., Yu, W., Shen, B., Sha, X., Dong, H., Huang, J., Wang, L., Zhu, W. and Xu, W. (2021) 'Lymph node metastasis-derived gastric cancer cells educate bone marrow-derived mesenchymal stem cells via YAP signaling activation by exosomal Wnt5a', *Oncogene,* 40(12), pp. 2296-2308.

Wang, X. Y., Zhu, W. W., Wang, Z., Huang, J. B., Wang, S. H., Bai, F. M., Li, T. E., Zhu, Y., Zhao, J., Yang, X., Lu, L., Zhang, J. B., Jia, H. L., Dong, Q. Z., Chen, J. H., Andersen, J. B.,

Disease Models & Mechanisms • DMM • Accepted manuscript

Ye, D. and Qin, L. X. (2022) 'Driver mutations of intrahepatic cholangiocarcinoma shape clinically relevant genomic clusters with distinct molecular features and therapeutic vulnerabilities', *Theranostics,* 12(1), pp. 260-276.

Yoshikawa, D., Ojima, H., Iwasaki, M., Hiraoka, N., Kosuge, T., Kasai, S., Hirohashi, S. and Shibata, T. (2008) 'Clinicopathological and prognostic significance of EGFR, VEGF, and HER2 expression in cholangiocarcinoma', *British Journal of Cancer,* 98(2), pp. 418-425.

Yuan, Z., Li, Y., Zhang, S., Wang, X., Dou, H., Yu, X., Zhang, Z., Yang, S. and Xiao, M. (2023) 'Extracellular matrix remodeling in tumor progression and immune escape: from mechanisms to treatments', *Mol Cancer,* 22(1), pp. 48.

Zhang, M., Yang, H., Wan, L., Wang, Z., Wang, H., Ge, C., Liu, Y., Hao, Y., Zhang, D., Shi, G., Gong, Y., Ni, Y., Wang, C., Zhang, Y., Xi, J., Wang, S., Shi, L., Zhang, L., Yue, W., Pei, X., Liu, B. and Yan, X. (2020) 'Single-cell transcriptomic architecture and intercellular crosstalk of human intrahepatic cholangiocarcinoma', *Journal of Hepatology,* 73(5), pp. 1118-1130.

Disease Models & Mechanisms • DMM • Accepted manuscript

Figures

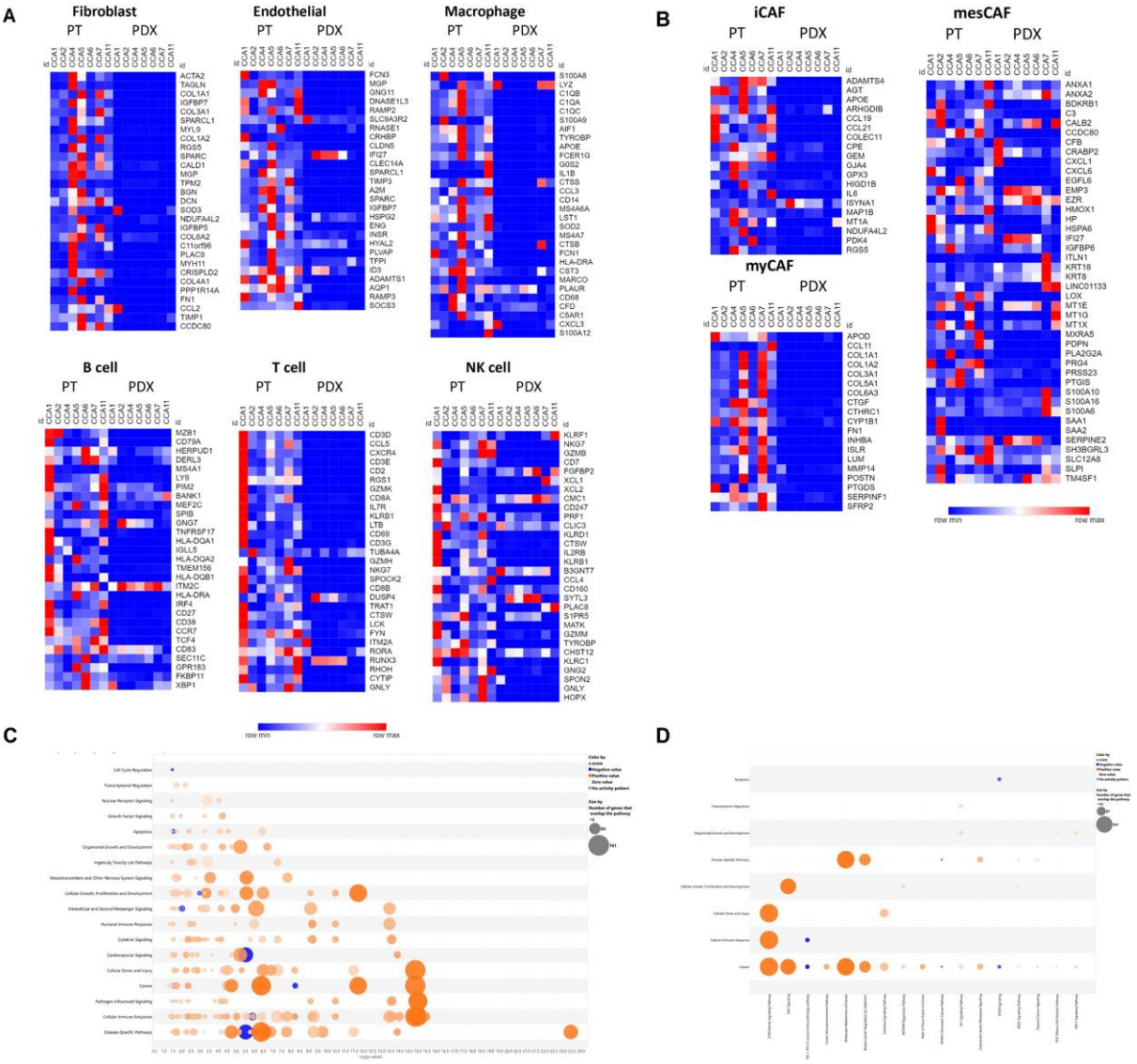

Fig. 1. Loss of Human Stromal Cells and Dysregulation of Cancer-Associated Pathways in CCA PDXs. Heatmaps of genes identified as being associated with different populations of stromal cells **(A)** or cancer-associated fibroblasts (**B**) through single-cell analysis (references 21 and 9 respectively) - iCAFs: immune-related CAFs, myCAF: myofibroblast-like CAFs, mesCAF: mesenchymal CAFs; blue and red indicate down- and up-regulated genes respectively. Bubble charts showing canonical pathways associated with signalling (**C**) or with cancer (**D**) that were significantly dysregulated comparing patient tissues to PDXs; orange and blue bubbles indicate activated and inhibited pathways respectively and the size of the bubble indicates the number of genes in each gene set.

Disease Models & Mechanisms • DMM • Accepted manuscript

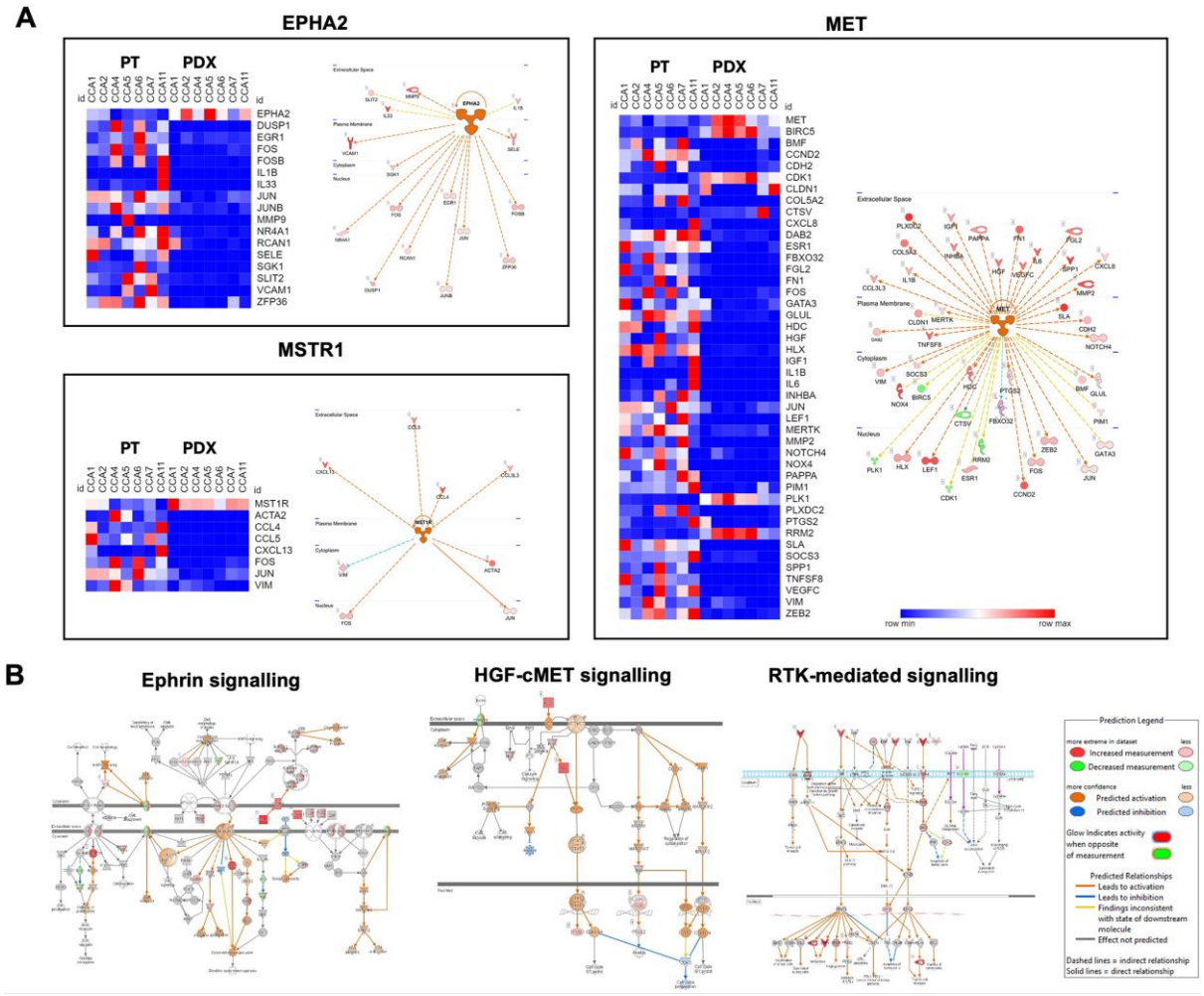

Fig. 2. Dysregulation of Paracrine Signalling Pathways in Cancer Cells Within CCA PDXs. Heatmaps (**A**) of genes involved in the pathways downstream of the top 3 ICAKs (kinases predicted to be inhibited in the PDXs in spite of maintained expression), MET, EPHA2 and MSTR1 and diagrams of the respective networks; blue and red indicate down- and up-regulated genes respectively. Diagrams of 3 pathways involving these and other kinases **(B**). Pathways are provided by Qiagen Ingenuity Pathway Analysis and were overlaid with information to demonstrate molecules which were over or underexpressed and/or predicted to be activated/inhibited in the patient tissues compared to the PDXs.

Disease Models & Mechanisms • DMM • Accepted manuscript

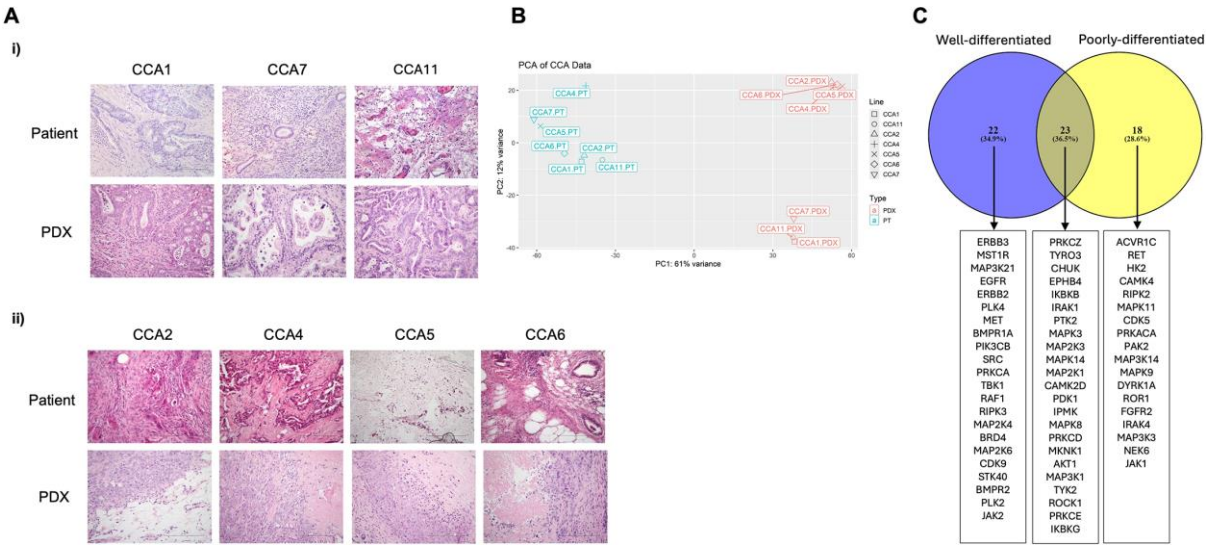

Fig. 3. Classification and Dysregulation of Upstream Regulators in CCA PDXs. Histology and Upstream Regulator analysis for two PDX subtypes. H&E staining of patient and PDX tissues (**A**) for two subtypes of PDXs: well-differentiated (**Ai**) and poorly-differentiated (**Aii**). PCA plot based on gene expression of patient and PDX samples, indicating two clusters of PDXs (**B**). Venn diagram to illustrate ICAKs found to be common or unique to the two PDX subtypes (**C**).

Disease Models & Mechanisms • DMM • Accepted manuscript

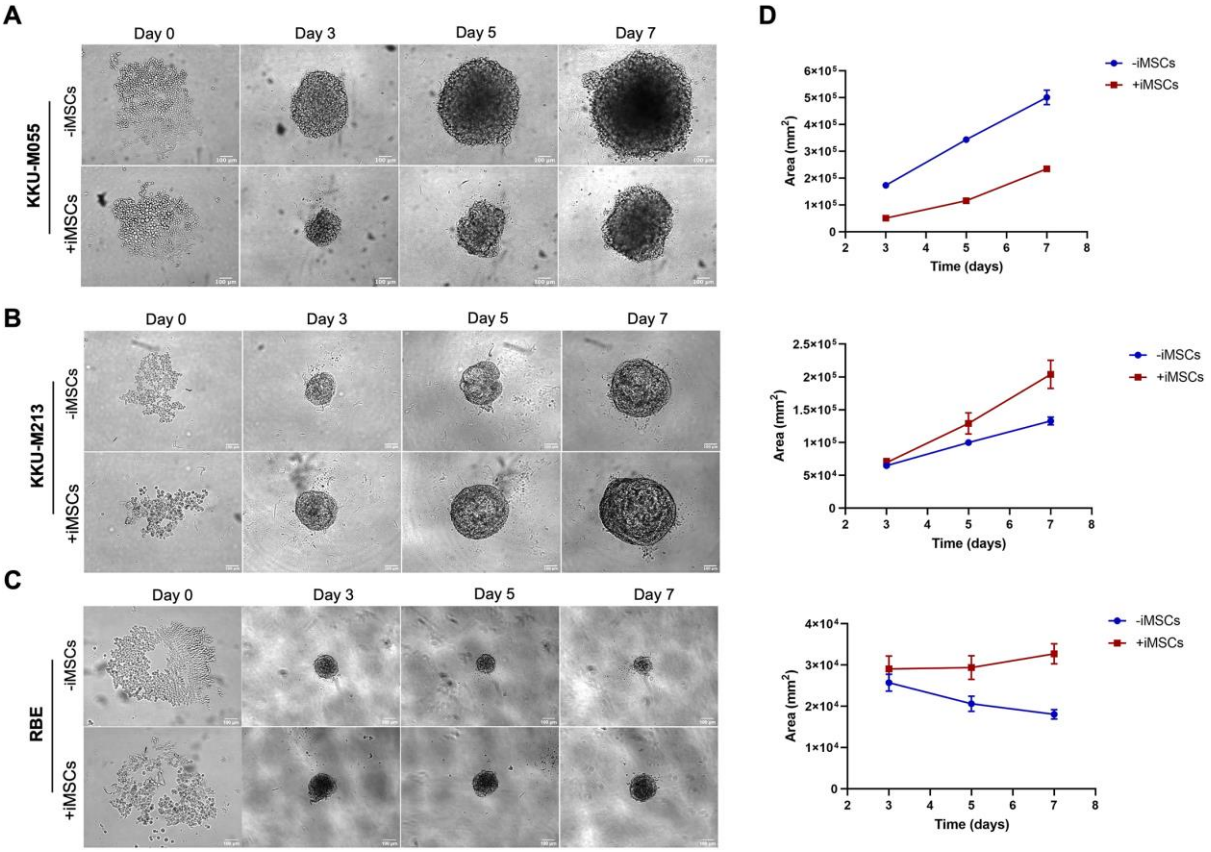

Fig. 4. Effect of iMSCs on CCA cells in spheroid co-culture. CCA cells (KKU-M055 **(A),** KKU-M213 **(B)** and RBE **(C))** were cultured as spheroids alone (monoculture) or iMSCs at a 1:2 ratio (cancer cells:iMSCs) (co-culture) into an ULA 96-well round bottom plate at a final cell density of 1000 cells per well with 100µg/ml of basement membrane extract (BME). The effect of co- culture with iMSCs was assessed using brightfield microscopy at day 0, 3, 5 and 7 at 1Ox magnification. Representative spheroids are shown. Scale bar 1OOµm. The spheroids were analysed after initiation to determine area based on image analysis of brightfield micrographs captured at each timepoint from three independent replicates (Mean ± SEM).

Disease Models & Mechanisms • DMM • Accepted manuscript

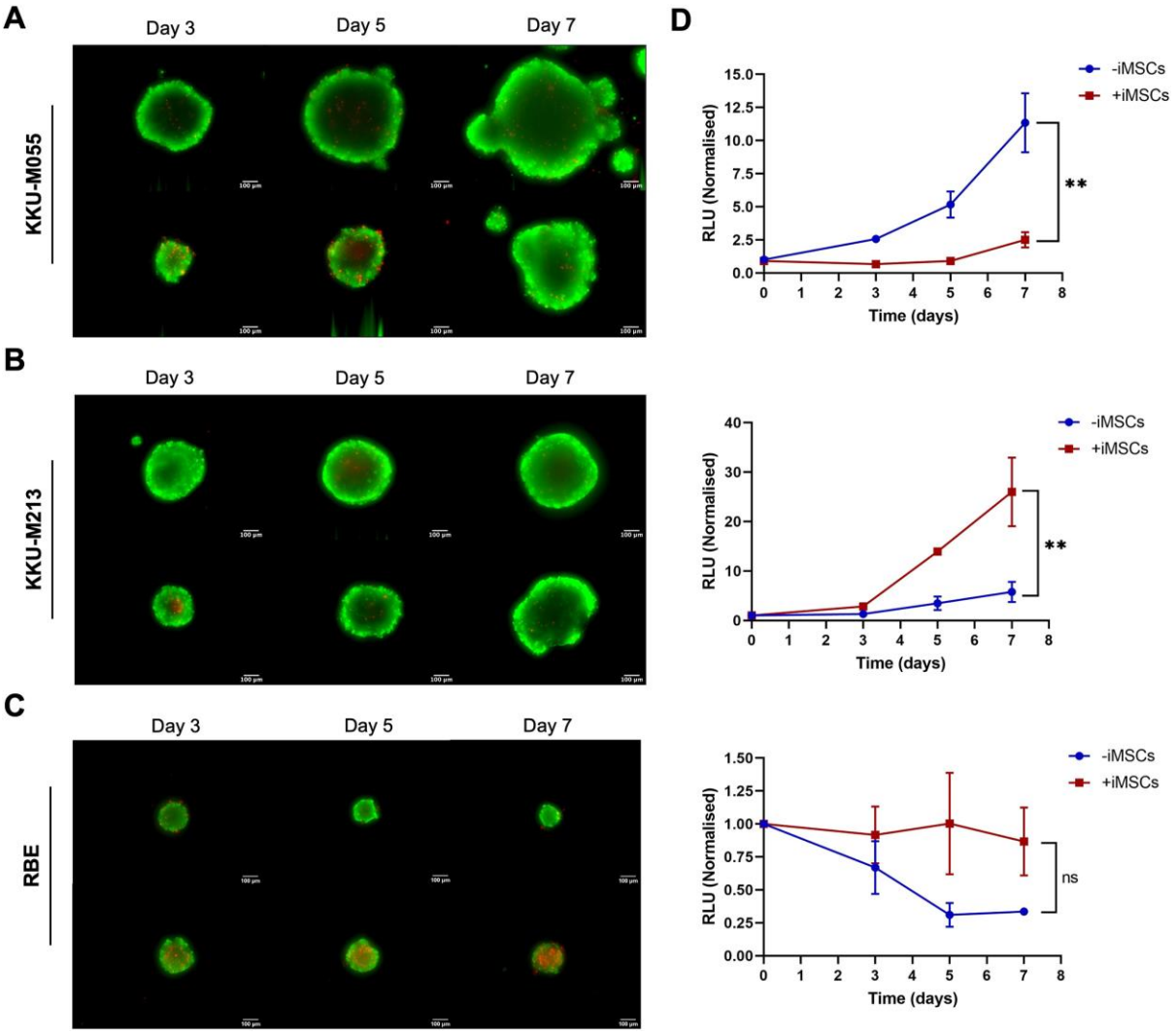

Fig. 5. Cell viability of CCA spheroids as monocultures and iMSC co-cultures. CCA cells (KKU-M055 (A), KKU-M213 (B) and RBE (C)) were cultured as spheroids alone (monoculture) or iMSCs at a 1:2 ratio (cancer cells:iMSCs) (co-culture) into an ULA 96-well round bottom plate at a final cell density of 1000 cells per well with 100µg/mL of basement membrane extract (BME). Live/dead cell staining was carried out using Calcein acetoxymethyl (AM) (green - live cells staining) and EthD-1 (red - dead cells staining) at days 3, 5 and 7. Representative spheroids are shown. Scale bar 100µm. Progressive growth of the spheroid was monitored by adding D-luciferin at day 0, 3, 5 and 7. Values were normalised to day 0 (Mean ± SEM). Co-cultures were compared to the monoculture via paired t-test (N=2) ns($p>0.05$), *($p<0.05$) and ****($p<0.0001$).

Disease Models & Mechanisms • DMM • Accepted manuscript

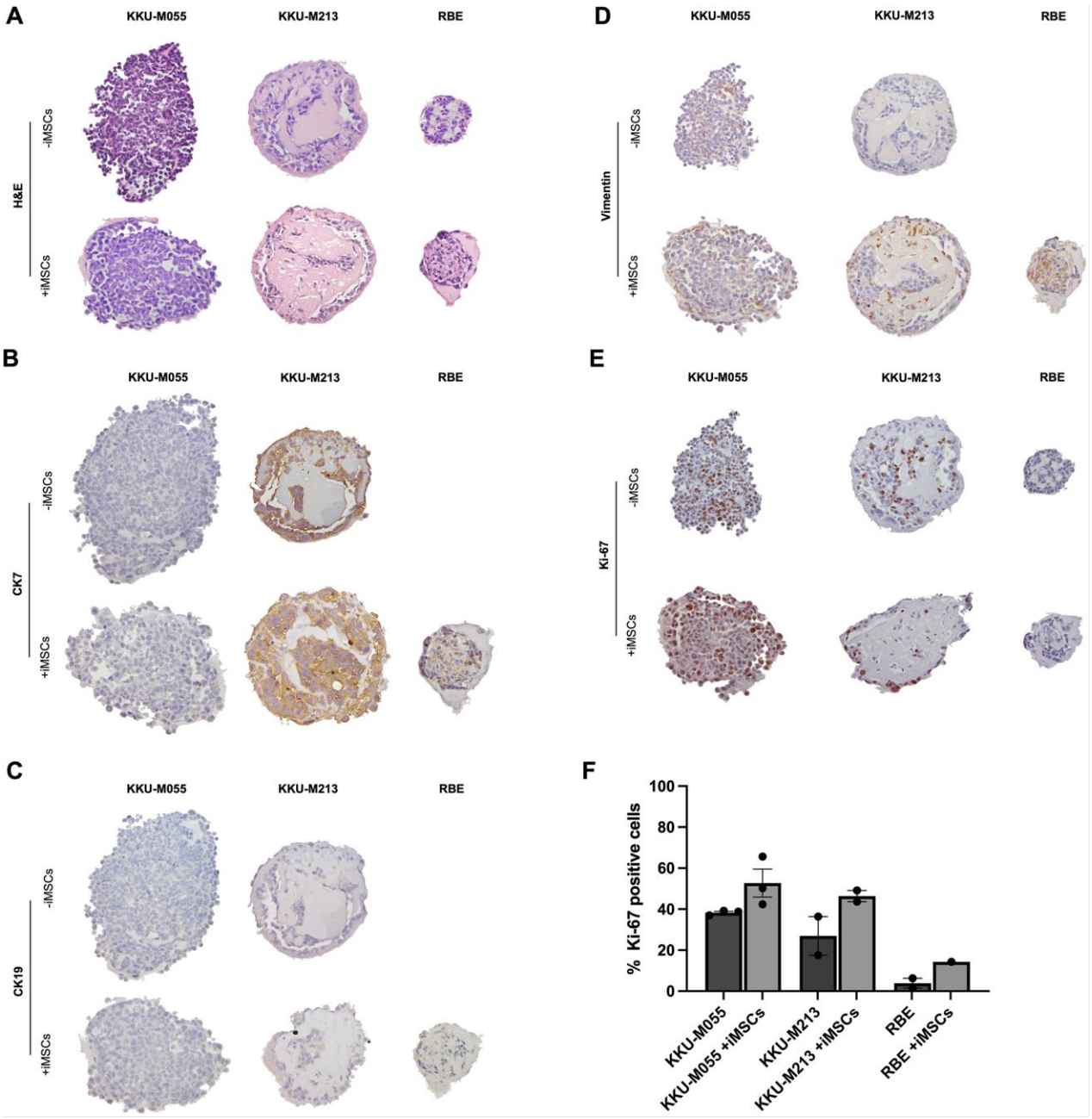

Fig. 6. Morphology and protein expression of the CCA spheroids. CCA cells (KKU-M055, KKU-M213 and RBE) were cultured as spheroids alone (monoculture) or iMSCs at a 1:2 (cancer cells:iMSCs) ratio (co-culture) into an ULA 96-well round bottom plate at a final cell density of 1000 cells per well with 100µg/mL of basement membrane extract (BME). The spheroids were fixed at day 5 of culture, paraffin embedded, sectioned, and stained with H&E (**A**), CK7 (**B**), CK19 (**C**), Vimentin (**D**) and Ki-67 (**E**). For Ki-67 staining, positive Ki-67 expression was quantified (**F**) by

Disease Models & Mechanisms • DMM • Accepted manuscript

manually counting the positive cells and cancer cells and calculating the ratio of positively stained cancer cells over the total of cancer cells. At least 6 spheroids were embedded in the array from each condition. Representative spheroids are shown at 20x magnification.

Disease Models & Mechanisms • DMM • Accepted manuscript

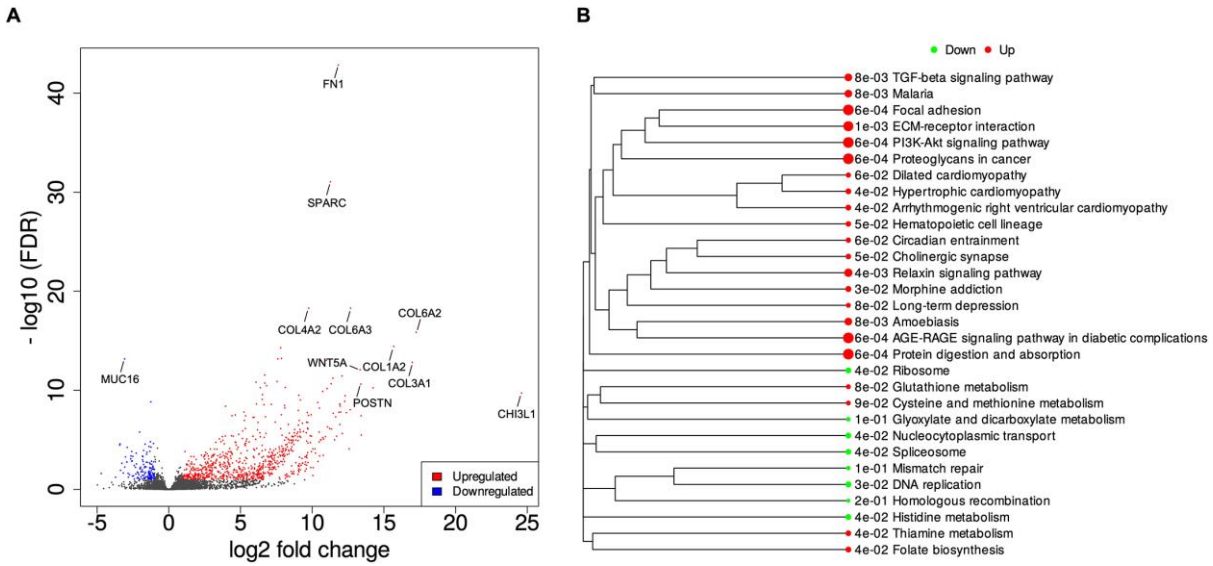

Fig. 7. Differential expression analysis using DESeq2 for the KKU-M213-derived spheroids. The differential expressed genes between monoculture and iMSCs co-culture were separated based on their FDR and fold change in a Volcano plot. The upregulated and downregulated genes were despite in red and blue, respectively (**A**). A gene set enrichment analysis (GSEA) was performed and KEGG-enrichment plots of representative gene sets from activated pathway were shown. The vertical items are the names of KEGG terms, and the downregulated and upregulated pathways are represented in green and red, respectively. the length of horizontal graph represents the gene ratio. The area of circle in the graph represents the fold-change value (**B**). These graphs were generated using IDEP.

Disease Models & Mechanisms • DMM • Accepted manuscript

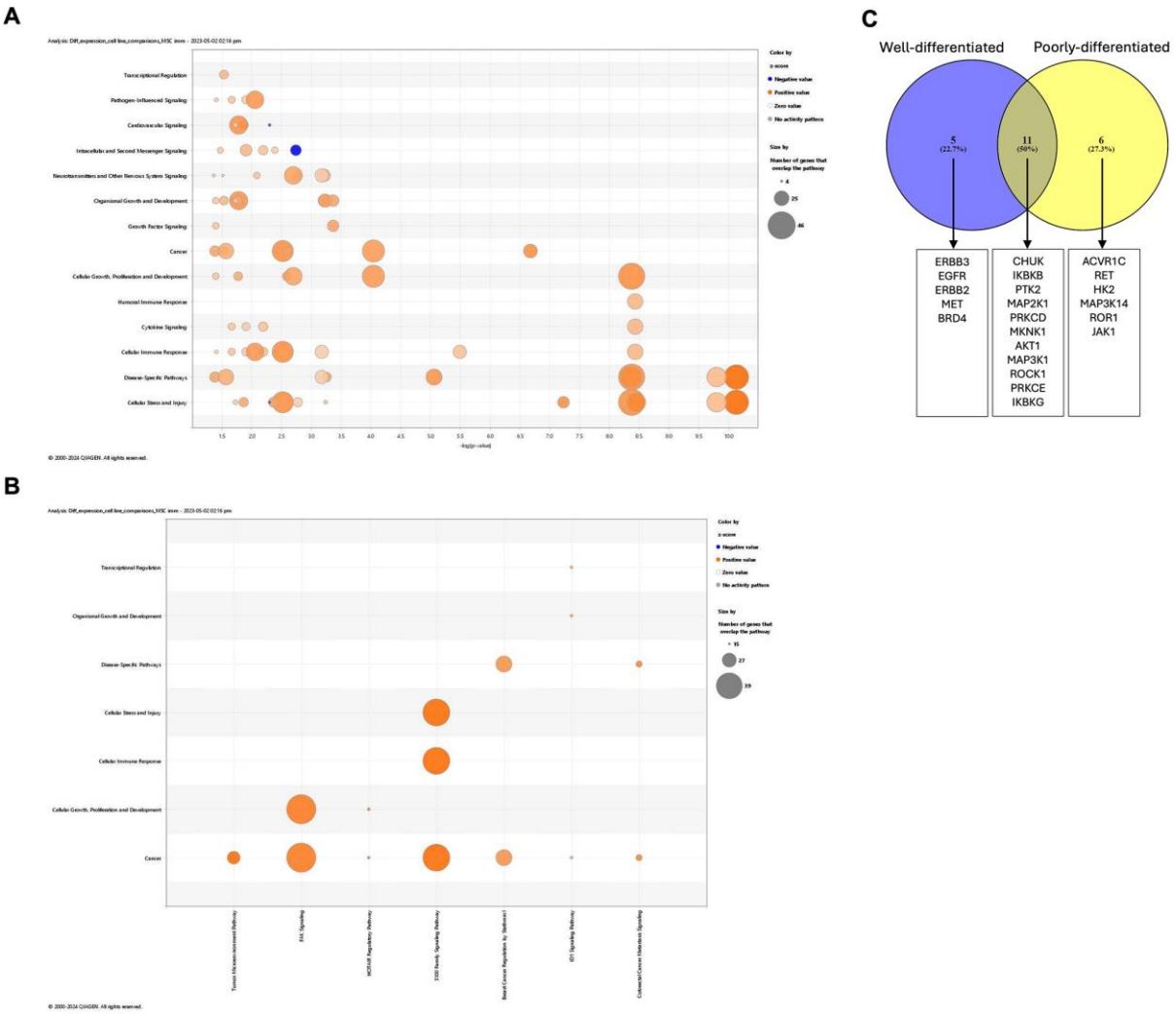

Fig. 8. Activation of ICAKs in MSC Co-Cultures and Restoration of POX-type Specific Signalling Pathways. Bubble charts showing canonical pathways associated with signalling **(A)** or with cancer **(B)** that were significantly activated in co-culture compared with monoculture spheroids; orange and blue bubbles indicate activated and inhibited pathways respectively and the size of the bubble indicates the number of genes in each geneset. Venn diagram to indicate ICAKs common to or unique to well- or poorly-differentiated PDXs, which were predicted to be activated in the co-culture compared to the monoculture spheroids **(C).**

Disease Models & Mechanisms • DMM • Accepted manuscript

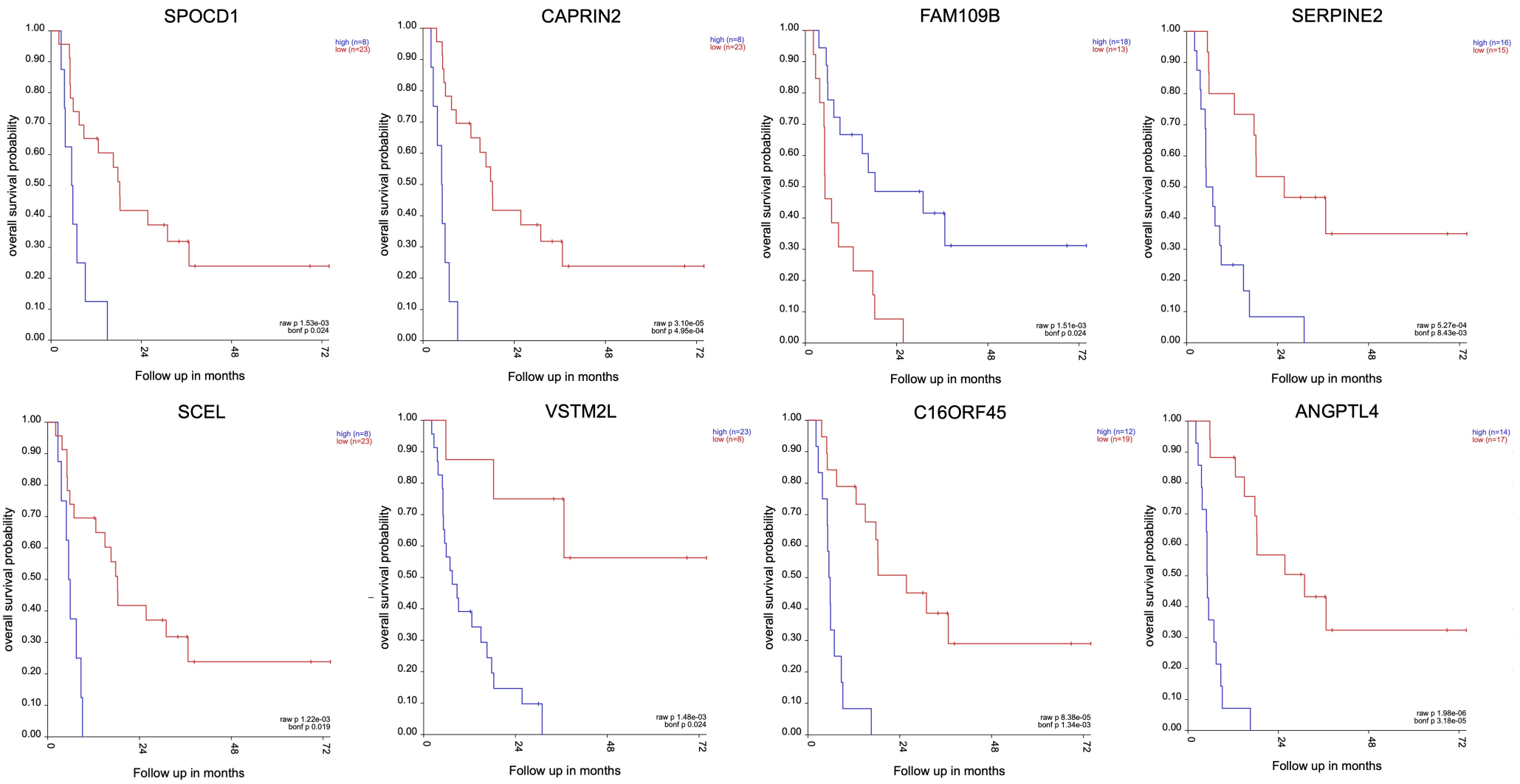

Fig. S1. Kaplan-Meier Survival Analysis of Genes Differentially Expressed in Co-Culture Model. Kaplan-Meier survival analysis was performed to assess the impact of gene expression on overall survival using dataset GSE89749 (33). The analysis focused on a subset of samples from patients with anatomic subtype, intrahepatic location, and fluke positive status to match the characteristics of KKU-M213.

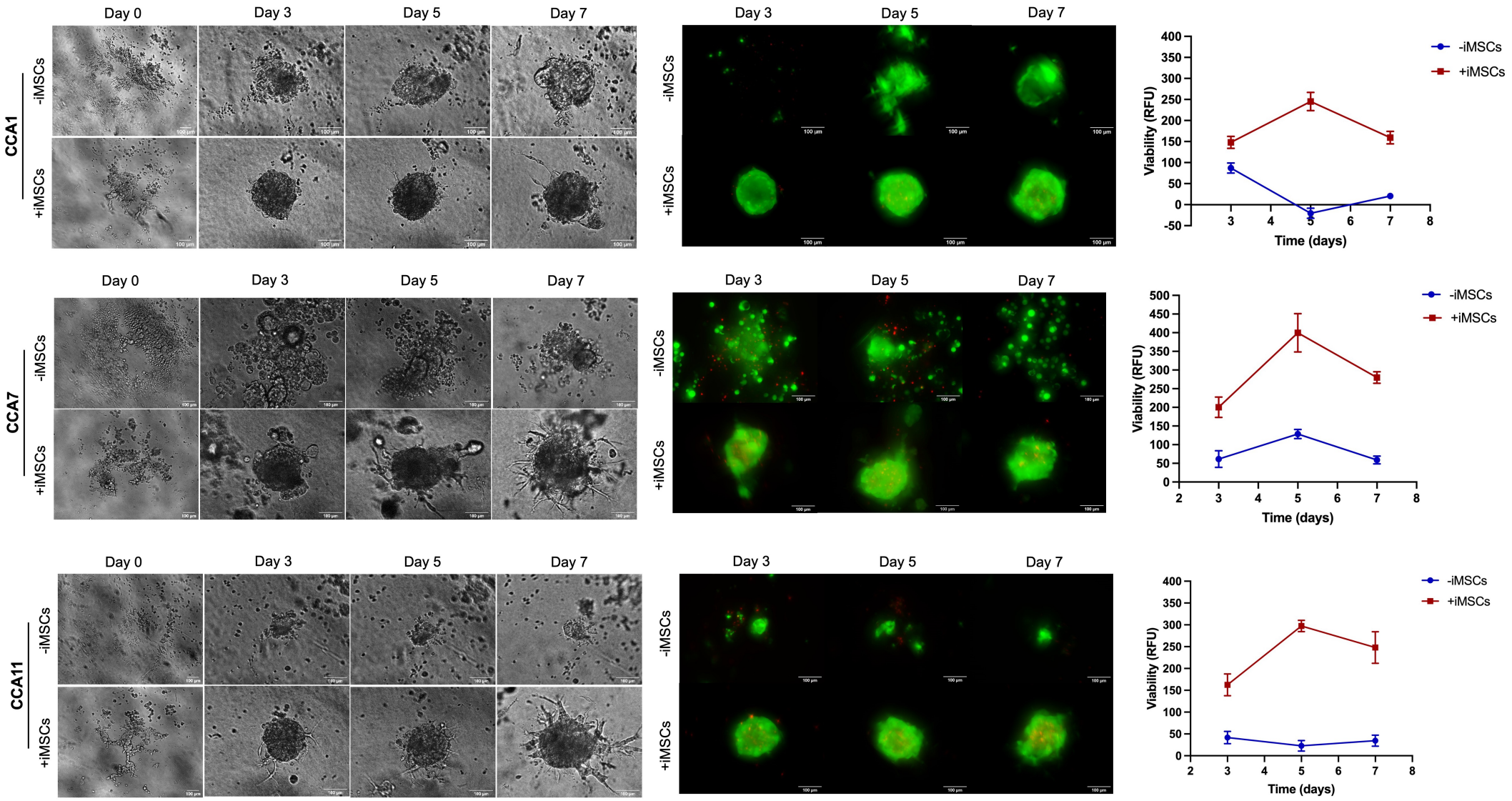

Fig. S3. Well-differentiated PDX-derived spheroids as monocultures and iMSCs co-cultures. CCA tissues (CCA1 (A), CCA7 (B) and CCA11 (C)) were enzymatically dissociated, and the cells were mono- or iMSCs co-cultured at 1:2 ratio (cancer cells:iMSCs) into an ULA 96-well round bottom plate at a final cell density of 1000 cells per well with 300µg/mL of basement membrane extract (BME). The effect of co-culture with iMSCs was assessed using brightfield microscopy at day 0, 3, 5 and 7 at 10x magnification. Live/dead cell staining was carried out using Calcein acetoxymethyl (AM) (green - live cells staining) and EthD-1 (red - dead cells staining) at days 3, 5 and 7. Representative spheroids are shown. Scale bar 100µm.

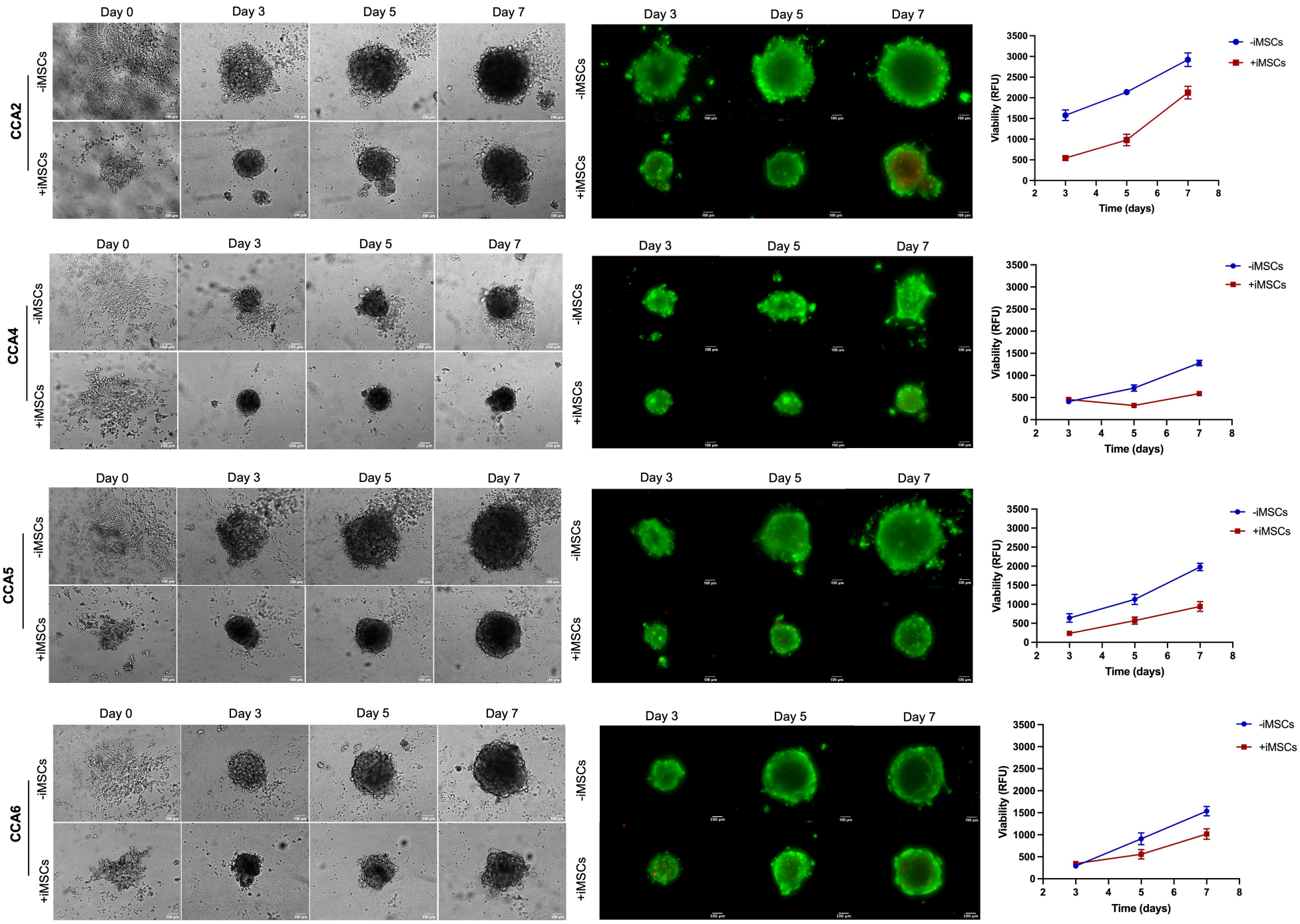

Fig. S2. Poorly-Differentiated PDX-derived spheroids as monocultures and iMSCs co-cultures. CCA tissues (CCA2 (A), CCA4 (B), CCA5 (C) and CCA6 (D)) were enzymatically dissociated, and the cells were mono- or iMSCs co-cultured at 1:2 ratio (cancer cells:iMSCs) into an ULA 96-well round bottom plate at a final cell density of 1000 cells per well with 300µg/mL of basement membrane extract (BME). The effect of co-culture with iMSCs was assessed using brightfield microscopy at day 0, 3, 5 and 7 at 10x magnification. Live/dead cell staining was carried out using Calcein acetoxymethyl (AM) (green - live cells staining) and EthD-1 (red - dead cells staining) at days 3, 5 and 7. Representative spheroids are shown. Scale bar 100µm. Viability was monitored by PrestoBlue at day 3, 5 and 7 (Mean ± SEM).

Table S1. Canonical pathways associated with cancer that were significantly dysregulated comparing patient tissues to PDXs.

Ingenuity Canonical Pathways	-log(p-value)	Ratio	z-score
S100 Family Signaling Pathway	14.9	0.28	9.54
FAK Signaling	11.7	0.27	9.70
PD-1, PD-L1 cancer immunotherapy pathway	8.25	0.40	-3.53
Tumor Microenvironment Pathway	6.39	0.31	5.98
Molecular Mechanisms of Cancer	6.38	0.22	9.99
Breast Cancer Regulation by Stathmin1	4.74	0.23	8.63
Cachexia Signaling Pathway	4.5	0.24	4.57
HOTAIR Regulatory Pathway	2.43	0.24	2.83
Role of Tissue Factor in Cancer	2.34	0.22	6.03
SPINK1 Pancreatic Cancer Pathway	2.31	0.33	-3.05
ID1 Signaling Pathway	1.71	0.21	2.60
Colorectal Cancer Metastasis Signaling	1.7	0.20	5.28
PTEN Signaling	1.53	0.21	-2.68
BEX2 Signaling Pathway	1.46	0.24	2.00
Thyroid Cancer Signaling	1.45	0.24	3.15
PCP (Planar Cell Polarity) Pathway	1.42	0.25	2.31
HEY1 Signaling Pathway	1.3	0.21	2.41

Table S2. List of Upstream Regulators identified through Ingenuity Pathway Analysis (IPA) Analysis, Including Growth Factors (GF), Cytokines, Kinases, and Transcription Regulators (TR).

Available for download at
https://journals.biologists.com/dmm/article-lookup/doi/10.1242/dmm.050716#supplementary-data

Table S3. Inhibited Cancer-Associated Kinases (ICAKs) identified in PDX Models.

Upstream Regulator	Expr Log Ratio	Expression (PDX vs PT)	Molecule Type	Predicted Activation State	Activation z-score	p-value of overlap
EPHA2	-1.94	3.85	kinase	Activated	2.16	6.34E-05
MET	-1.88	3.69	kinase	Activated	3.19	3.60E-08
MST1R	-1.72	3.29	kinase	Activated	2.80	6.54E-03
MAP3K21	-1.66	3.16	kinase	Activated	2.00	2.26E-02
TYRO3	-1.52	2.87	kinase	Activated	2.41	3.72E-06
PRKCZ	-1.35	2.55	kinase	Activated	3.39	6.32E-04
EIF2AK2	-1.05	2.07	kinase	Activated	3.21	1.54E-02
RET	-0.97	1.95	kinase	Activated	2.28	2.15E-07
CHUK	-0.87	1.83	kinase	Activated	6.10	6.93E-19
CDK6	-0.82	1.76	kinase	Activated	2.24	7.59E-02
CAMK2D	-0.66	1.58	kinase	Activated	2.00	2.56E-02
CDK5	-0.62	1.53	kinase	Activated	2.76	1.11E-05
EPHB4	-0.47	1.38	kinase	Activated	3.19	2.77E-03
PTK2	-0.44	1.35	kinase	Activated	3.45	2.42E-07
PAK1	-0.31	1.24	kinase	Activated	2.21	2.55E-01
IRAK1	-0.31	1.24	kinase	Activated	2.36	4.68E-04
TBK1	-0.29	1.22	kinase	Activated	3.03	7.47E-04
PDK1	-0.27	1.20	kinase	Activated	4.23	6.01E-03
MAP2K3	-0.23	1.17	kinase	Activated	3.26	3.58E-03
MAP2K1	-0.18	1.13	kinase	Activated	3.51	1.29E-11
RIPK2	-0.11	1.08	kinase	Activated	5.39	1.54E-04
MAPK8	-0.08	1.05	kinase	Activated	4.22	2.22E-08
MAPK9	-0.03	1.02	kinase	Activated	2.90	1.33E-06
MAPK14	-0.02	1.01	kinase	Activated	4.48	1.51E-18
PRKACA	0.07	0.95	kinase	Activated	2.03	2.18E-04
HK2	0.09	0.94	kinase	Activated	2.24	1.52E-01
IKBKG	0.10	0.93	kinase	Activated	4.97	1.34E-13
SRC	0.10	0.93	kinase	Activated	2.29	1.94E-07
RPS6KA5	0.11	0.93	kinase	Activated	2.12	3.34E-04
MAPK11	0.12	0.92	kinase	Activated	2.81	1.25E-02
RAF1	0.15	0.90	kinase	Activated	2.94	3.33E-06
IPMK	0.16	0.90	kinase	Activated	4.12	7.18E-06
PRKCD	0.19	0.88	kinase	Activated	3.61	3.43E-08
TYK2	0.20	0.87	kinase	Activated	3.02	4.09E-08
CDK9	0.23	0.85	kinase	Activated	2.79	2.66E-09
AKT1	0.25	0.84	kinase	Activated	2.60	2.81E-18
MAPK3	0.26	0.84	kinase	Activated	4.07	3.93E-08
ROCK1	0.28	0.83	kinase	Activated	3.97	9.44E-08
IKBKB	0.31	0.80	kinase	Activated	6.44	1.25E-26
MAP3K14	0.37	0.78	kinase	Activated	3.12	1.68E-07
DYRK1A	0.39	0.77	kinase	Activated	2.31	1.18E-05
PRKCE	0.46	0.72	kinase	Activated	3.60	1.37E-07
MAP3K1	0.49	0.71	kinase	Activated	2.81	1.35E-04
MKNK1	0.65	0.64	kinase	Activated	4.80	5.93E-05
ROR1	0.77	0.58	kinase	Activated	3.20	3.20E-03
CAMK4	0.79	0.58	kinase	Activated	2.77	1.77E-03

Table S4. Upstream Regulators and Inhibited Cancer-Associated Kinases (ICAKs) identified in the Well-Differentiated group.

Upstream Regulator	Expr Log Ratio	Expression (PDX vs PT)	Molecule Type	Predicted Activation State	Activation z-score	p-value of overlap
ACVR1C	4.72	26.32	kinase	Inhibited	2.43	9.12E-02
RET	1.91	3.76	kinase	Inhibited	3.13	2.15E-07
HK2	1.71	3.27	kinase	Inhibited	2.00	3.72E-01
TYRO3	1.65	3.13	kinase	Inhibited	2.20	2.79E-03
CAMK2D	1.38	2.61	kinase	Inhibited	2.00	4.02E-02
CHUK	1.29	2.44	kinase	Inhibited	5.13	5.97E-15
PRKCZ	1.24	2.36	kinase	Inhibited	2.60	1.40E-02
CAMK4	1.06	2.09	kinase	Inhibited	3.23	1.24E-03
RIPK2	1.04	2.06	kinase	Inhibited	2.94	4.52E-05
MAPK11	0.94	1.92	kinase	Inhibited	2.16	7.27E-03
CDK5	0.90	1.87	kinase	Inhibited	2.27	2.13E-04
PDK1	0.76	1.69	kinase	Inhibited	3.13	2.10E-03
PTK2	0.71	1.64	kinase	Inhibited	3.17	1.25E-06
IKBKG	0.71	1.63	kinase	Inhibited	4.76	1.44E-11
EPHB4	0.59	1.51	kinase	Inhibited	2.85	6.43E-04
PRKACA	0.53	1.44	kinase	Inhibited	2.44	3.82E-05
MAP2K1	0.53	1.44	kinase	Inhibited	2.69	3.60E-14
MAPK8	0.49	1.41	kinase	Inhibited	2.87	8.35E-10
PAK2	0.48	1.39	kinase	Inhibited	2.14	5.61E-04
IRAK1	0.46	1.38	kinase	Inhibited	2.46	8.17E-03
MAP3K14	0.45	1.37	kinase	Inhibited	3.29	5.94E-06
MAP2K3	0.43	1.35	kinase	Inhibited	3.04	7.86E-04
TYK2	0.16	1.12	kinase	Inhibited	3.58	1.86E-05
MAPK9	0.11	1.08	kinase	Inhibited	3.11	8.74E-05
ROCK1	0.08	1.05	kinase	Inhibited	3.45	4.83E-07
MAPK14	0.07	1.05	kinase	Inhibited	3.86	3.85E-16
AKT1	0.05	1.04	kinase	Inhibited	2.50	1.31E-17
IPMK	0.05	1.04	kinase	Inhibited	3.18	2.86E-03
PRKCD	0.05	1.03	kinase	Inhibited	3.38	3.94E-09
DYRK1A	0.04	1.03	kinase	Inhibited	2.44	3.40E-03
PRKCE	-0.13	0.91	kinase	Inhibited	2.73	2.21E-04
ROR1	-0.19	0.88	kinase	Inhibited	2.20	6.10E-03
FGFR2	-0.34	0.79	kinase	Inhibited	2.31	2.45E-08
MAP3K1	-0.35	0.79	kinase	Inhibited	2.22	7.86E-04
IRAK4	-0.46	0.73	kinase	Inhibited	2.12	4.36E-03
MAPK3	-0.48	0.72	kinase	Inhibited	2.57	3.04E-05
MAP3K3	-0.62	0.65	kinase	Inhibited	2.39	5.41E-06
IKBKB	-0.64	0.64	kinase	Inhibited	5.93	1.52E-18
MKNK1	-0.67	0.63	kinase	Inhibited	2.44	6.20E-04
NEK6	-0.84	0.56	kinase	Inhibited	2.00	3.35E-02
JAK1	-0.92	0.53	kinase	Inhibited	2.68	1.24E-02

Table S5. Upstream Regulators and Inhibited Cancer-Associated Kinases (ICAKs) identified in the Poorly-Differentiated group.

Upstream Regulator	Expr Log Ratio	Expression (PDX vs PT)	Molecule Type	Predicted Activation State	Activation z-score	p-value of overlap
ERBB3	2.67	6.38	kinase	Inhibited	2.154	5.73E-13
MST1R	2.21	4.62	kinase	Inhibited	2.449	3.81E-03
MAP3K21	2.15	4.45	kinase	Inhibited	2	1.46E-03
EGFR	2.14	4.41	kinase	Inhibited	2.213	5.51E-06
ERBB2	2.11	4.33	kinase	Inhibited	3.731	1.01E-11
PRKCZ	1.57	2.97	kinase	Inhibited	2.774	1.75E-03
TYRO3	1.44	2.71	kinase	Inhibited	2.412	2.30E-06
PLK4	1.16	2.24	kinase	Inhibited	2.449	5.06E-03
MET	1.16	2.24	kinase	Inhibited	4.548	2.48E-06
BMPR1A	0.90	1.86	kinase	Inhibited	2.207	1.31E-02
PIK3CB	0.75	1.68	kinase	Inhibited	2.216	4.11E-04
SRC	0.46	1.38	kinase	Inhibited	2.619	8.84E-10
PRKCA	0.42	1.34	kinase	Inhibited	2.674	1.09E-03
CHUK	0.40	1.32	kinase	Inhibited	5.426	3.62E-15
EPHB4	0.39	1.31	kinase	Inhibited	2.764	4.37E-03
IKBKB	0.32	1.25	kinase	Inhibited	5.692	3.33E-22
IRAK1	0.19	1.14	kinase	Inhibited	2.036	1.03E-03
PTK2	0.16	1.12	kinase	Inhibited	3.063	9.14E-09
MAPK3	0.15	1.11	kinase	Inhibited	2.742	1.67E-06
TBK1	0.05	1.03	kinase	Inhibited	3.575	1.67E-06
MAP2K3	0.04	1.02	kinase	Inhibited	2.95	1.28E-04
MAPK14	0.03	1.02	kinase	Inhibited	4.766	3.86E-18
RAF1	-0.05	0.97	kinase	Inhibited	3.985	1.27E-02
RIPK3	-0.07	0.95	kinase	Inhibited	2.4	2.01E-03
MAP2K4	-0.14	0.91	kinase	Inhibited	2.8	4.73E-02
MAP2K1	-0.20	0.87	kinase	Inhibited	4.861	6.11E-11
CAMK2D	-0.25	0.84	kinase	Inhibited	2	1.05E-02
PDK1	-0.29	0.82	kinase	Inhibited	3.162	3.84E-02
IPMK	-0.35	0.78	kinase	Inhibited	3.742	4.75E-05

MAPK8	-0.42	0.75	kinase	Inhibited	2.244	2.47E-06
PRKCD	-0.43	0.74	kinase	Inhibited	2.78	9.99E-03
BRD4	-0.44	0.74	kinase	Inhibited	4.838	8.29E-09
MAP2K6	-0.52	0.70	kinase	Inhibited	2.183	1.30E-08
MKNK1	-0.53	0.69	kinase	Inhibited	4.214	5.90E-05
AKT1	-0.56	0.68	kinase	Inhibited	4.292	1.15E-12
MAP3K1	-0.59	0.67	kinase	Inhibited	2.477	4.20E-04
TYK2	-0.61	0.65	kinase	Inhibited	2.688	2.08E-06
CDK9	-0.62	0.65	kinase	Inhibited	2.415	2.95E-07
STK40	-0.63	0.65	kinase	Inhibited	3.138	7.79E-08
ROCK1	-0.64	0.64	kinase	Inhibited	3.719	3.41E-09
BMPR2	-0.81	0.57	kinase	Inhibited	2.413	2.62E-02
PLK2	-0.83	0.56	kinase	Inhibited	2.236	2.30E-02
PRKCE	-0.84	0.56	kinase	Inhibited	3.264	1.13E-02
IKBKG	-0.88	0.54	kinase	Inhibited	4.302	9.31E-07
JAK2	-0.88	0.54	kinase	Inhibited	2.201	8.79E-08

Table S6. Genes differentially expressed in the co-culture model associated with overall survival. The adjusted p-values were derived from Kaplan-Meier survival analysis using Cox proportional regression. Additionally, the log2 difference in expression in the co-culture is provided for each gene.

Gene Symbol	Adjusted p-value	Log2 Fold Change in Expression in Co-culture
SPOCD1	0.024	2.241128
CAPRIN2	4.95E-04	1.233663
FAM109B	0.024	9.388593
SERPINE2	8.43E-03	2.074787
SCEL	0.019	-1.55945
VSTM2L	0.024	6.567292
C16ORF45	1.30E-03	6.774376
ANGPTL4	3.20E-05	1.230297

Table S7. Differentially expressed genes identified by DESeq2 in KKU-M213-derived spheroids (monoculture vs co-culture). Gene ID, name, adjusted p-value, and log2-fold change are provided for each gene.

Available for download at
https://journals.biologists.com/dmm/article-lookup/doi/10.1242/dmm.050716#supplementary-data

Table S8. Inhibited Cancer-Associated Kinases (ICAKs) Activated in MSC Co-Cultures Identified from Whole PDX Analysis.

Upstream Regulator	Expr Log Ratio	Expression (PDX vs PT)	Molecule Type	Predicted Activation State	Activation z-score	p-value of overlap
EPHA2	-		-	-	-	-
MET	0.01	1.00	kinase	Activated	3.39	2.68E-06
MST1R	-		-	-	-	-
MAP3K21	-0.27	0.83	kinase			6.63E-03
TYRO3	-		-	-	-	-
PRKCZ	-0.18	0.88	kinase		1.98	4.50E-02
EIF2AK2	-		-	-	-	-
RET			kinase	Activated	2.39	3.33E-05
CHUK	-0.01	0.99	kinase	Activated	3.06	2.57E-08
CDK6	-0.13	0.91	kinase		1.89	1.72E-01
CAMK2D	-		-	-	-	-
CDK5	-		-	-	-	-
EPHB4	-		-	-	-	-
PTK2	0.05	1.04	kinase	Activated	2.39	9.84E-08
PAK1	-		-	-	-	-
IRAK1	0.09	1.06	kinase		0.72	3.02E-02
TBK1	-		-	-	-	-
PDK1	-		-	-	-	-
MAP2K3	0.08	1.05	kinase		1.98	3.86E-06
MAP2K1	0.01	1.01	kinase	Activated	2.30	7.77E-07
RIPK2	-		-	-	-	-
MAPK8	-0.15	0.90	kinase		0.96	1.41E-04
MAPK9	-		-	-	-	-
MAPK14	0.14	1.10	kinase		1.71	3.27E-04
PRKACA	-		-	-	-	-
HK2	-0.82	0.57	kinase	Activated	2.22	1.06E-03
IKBKG	0.04	1.03	kinase	Activated	2.68	7.10E-06
SRC	0.08	1.05	kinase		1.41	1.58E-06
RPS6KA5	-		-	-	-	-

MAPK11	-		-	-	-	-
RAF1	-		-	-	-	-
IPMK	-0.26	0.84	kinase		1.22	7.53E-03
PRKCD	-0.19	0.88	kinase	Activated	2.47	7.00E-04
TYK2	-		-	-	-	-
CDK9	0.06	1.04	kinase			8.52E-03
AKT1	0.46	1.38	kinase	Activated	3.03	1.44E-06
MAPK3	-		-	-	-	-
ROCK1	0.20	1.15	kinase	Activated	3.44	1.98E-09
IKBKB	0.14	1.10	kinase	Activated	3.29	3.05E-10
MAP3K14	0.17	1.12	kinase	Activated	2.56	1.95E-04
DYRK1A	-		-	-	-	-
PRKCE	-0.22	0.86	kinase	Activated	2.60	1.05E-02
MAP3K1	-0.28	0.82	kinase	Activated	2.00	8.52E-03
MKNK1	-0.12	0.92	kinase	Activated	2.16	2.71E-03
ROR1	0.27	1.20	kinase	Activated	2.76	1.58E-03
CAMK4	-		-	-	-	-

Table S9. Inhibited Cancer-Associated Kinases (ICAKs) Activated in MSC Co-Cultures Identified from well-differentiated PDXs.

Upstream Regulator	Expr Log Ratio	Expression (PDX vs PT)	Molecule Type	Predicted Activation State	Activation z-score	p-value of overlap
ERBB3	-1.07		kinase	Activated	2.10	7.66E-11
MST1R	-	1.00	-	-	-	-
MAP3K21	-0.27		kinase			6.63E-03
EGFR	-0.10	0.83	kinase	Activated	2.73	9.69E-06
ERBB2	-0.29		kinase	Activated	2.75	1.92E-21
PRKCZ	-0.18	0.88	kinase		1.98	4.50E-02
TYRO3	-		-	-	-	-
PLK4	-		-	-	-	-
MET	0.01	0.99	kinase	Activated	3.39	2.68E-06
BMPR1A	-0.17	0.91	kinase		0.56	1.55E-03
PIK3CB	-		-	-	-	-
SRC	0.08		kinase		1.41	1.58E-06
PRKCA	-		-	-	-	-
CHUK	-0.01	1.04	kinase	Activated	3.06	2.57E-08
EPHB4	-		-	-	-	-
IKBKB	0.14	1.06	kinase	Activated	3.29	3.05E-10
IRAK1	0.09		kinase		0.72	3.02E-02
PTK2	0.05		kinase	Activated	2.39	9.84E-08
MAPK3	-	1.05	-	-	-	-
TBK1	-	1.01	-	-	-	-
MAP2K3	0.08		kinase		1.98	3.86E-06
MAPK14	0.14	0.90	kinase		1.71	3.27E-04
RAF1	-		-	-	-	-
RIPK3	0.15	1.10	kinase			4.10E-02
MAP2K4	-		-	-	-	-
MAP2K1	0.01	0.57	kinase	Activated	2.30	7.77E-07
CAMK2D	-	1.03	-	-	-	-
PDK1	-	1.05	-	-	-	-
IPMK	-0.26		kinase		1.22	7.53E-03

MAPK8	-0.15		kinase		0.96	1.41E-04
PRKCD	-0.19		kinase	Activated	2.47	7.00E-04
BRD4		0.84	kinase	Activated	3.50	7.45E-07
MAP2K6	-0.79	0.88	kinase		1.69	3.20E-04
MKNK1	-0.12		kinase	Activated	2.16	2.71E-03
AKT1	0.46	1.04	kinase	Activated	3.03	1.44E-06
MAP3K1	-0.28	1.38	kinase	Activated	2.00	8.52E-03
TYK2	-		-	-	-	-
CDK9	0.06	1.15	kinase			8.52E-03
STK40	-0.06	1.10	kinase		1.16	2.71E-04
ROCK1	0.20	1.12	kinase	Activated	3.44	1.98E-09
BMPR2	1.70		kinase		1.13	3.87E-02
PLK2	-	0.86	-	-	-	-
PRKCE	-0.22	0.82	kinase	Activated	2.60	1.05E-02
IKBKG	0.04	0.92	kinase	Activated	2.68	7.10E-06
JAK2	0.35	1.20	kinase		1.73	3.65E-03

Table S10. Inhibited Cancer-Associated Kinases (ICAKs) Activated in MSC Co-Cultures Identified from poorly-differentiated PDXs.

Upstream Regulator	Expr Log Ratio	Expression (PDX vs PT)	Molecule Type	Predicted Activation State	Activation z-score	p-value of overlap
ACVR1C	-1.32		kinase	Activated	2.61	2.94E-04
RET		1.00	kinase	Activated	2.39	3.33E-05
HK2	-0.82		kinase	Activated	2.22	1.06E-03
TYRO3	-	0.83	-	-	-	-
CAMK2D	-		-	-	-	-
CHUK	-0.01	0.88	kinase	Activated	3.06	2.57E-08
PRKCZ	-0.18		kinase		1.98	4.50E-02
CAMK4	-		-	-	-	-
RIPK2	-	0.99	-	-	-	-
MAPK11	-	0.91	-	-	-	-
CDK5	-		-	-	-	-
PDK1	-		-	-	-	-
PTK2	0.05		kinase	Activated	2.39	9.84E-08
IKBKG	0.04	1.04	kinase	Activated	2.68	7.10E-06
EPHB4	-		-	-	-	-
PRKACA	-	1.06	-	-	-	-
MAP2K1	0.01		kinase	Activated	2.30	7.77E-07
MAPK8	-0.15		kinase		0.96	1.41E-04
PAK2	-0.06	1.05	kinase		0.45	1.64E-02
IRAK1	0.09	1.01	kinase		0.72	3.02E-02
MAP3K14	0.17		kinase	Activated	2.56	1.95E-04
MAP2K3	0.08	0.90	kinase		1.98	3.86E-06
TYK2	-		-	-	-	-
MAPK9	-	1.10	-	-	-	-
ROCK1	0.20		kinase	Activated	3.44	1.98E-09
MAPK14	0.14	0.57	kinase		1.71	3.27E-04
AKT1	0.46	1.03	kinase	Activated	3.03	1.44E-06
IPMK	-0.26	1.05	kinase		1.22	7.53E-03
PRKCD	-0.19		kinase	Activated	2.47	7.00E-04

DYRK1A	-		-	-	-	-
PRKCE	-0.22		kinase	Activated	2.60	1.05E-02
ROR1	0.27	0.84	kinase	Activated	2.76	1.58E-03
FGFR2	-0.49	0.88	kinase		-0.08	4.77E-07
MAP3K1	-0.28		kinase	Activated	2.00	8.52E-03
IRAK4	-	1.04	-	-	-	-
MAPK3	-	1.38	-	-	-	-
MAP3K3	0.46		kinase			3.98E-03
IKBKB	0.14	1.15	kinase	Activated	3.29	3.05E-10
MKNK1	-0.12	1.10	kinase	Activated	2.16	2.71E-03
NEK6	-	1.12	-	-	-	-
JAK1	0.40		kinase	Activated	2.80	2.71E-03